LA-UR-12-25426
Approved for public release; distribution is unlimited.

Title:	Assessing the Effect of Parametric Uncertainty on the FRAPCON-3.4 Thermal Conductivity Model
Author(s):	Stull, Christopher J. Williams, Brian J. Unal, Cetin
Intended for:	Report

Assessing the Effect of Parametric Uncertainty on the FRAPCON-3.4 Thermal Conductivity Model

Christopher J. Stull[1], *Brian J. Williams*[2], *Cetin Unal*[3]

Los Alamos National Laboratory, Los Alamos, New Mexico 87545

Executive Summary

In the absence of a well-accepted, mathematical description of how units of material respond to one or more external actions, scientists must often rely upon empirically-derived models to make predictions. These models are often employed to model very complex phenomena, with an unfortunate side-effect that intuition, as to the values of particular model parameters, may not serve to guide their use. Given our increased reliance on modeling and simulation to make predictions in the absence of experimental data, it befits the scientific and engineering communities to explore and report upon uncertainty quantification techniques applied to previously adopted (or at least well-accepted) empirical models that derive from or pertain to substantial experimental data sets. This report represents a collection of three methodologies aimed at assessing the predictive capability of the empirical thermal conductivity model adopted by the nuclear fuel performance code, FRAPCON-3.4. Each of these methodologies considers the effect of uncertain parameters – a plausible reality in the context of empirically-derived models – on the ability of the model to predict uranium dioxide conductivity data from open literature sources. The results lead the authors to question the predictive capability of the FRAPCON model for predicting the thermal conductivities associated with *irradiated* fuel samples. The report concludes with a preliminary examination of *Idaho National Laboratory's* (INL) nuclear fuel performance code, BISON, developed under INL's *Multiphysics Object Oriented Simulation Environment* (MOOSE). ***(Approved for unlimited, public release on October XX, 2012, LA-UR-12-2XXXX, Unclassified)***

[1] Technical Staff Member in Applied Engineering and Technology Division (AET-6). Mailing: Los Alamos National Laboratory, PO Box 1663, MS P915, Los Alamos, New Mexico 87545. Phone: 505-667-7164. Email: stull@lanl.gov.

[2] Technical Staff Member in Computer, Computational, and Statistical Sciences Division (CCS-6). Mailing: Los Alamos National Laboratory, PO Box 1663, MS F600, Los Alamos, New Mexico 87545. Phone: 505-667-2331. Email: brianw@lanl.gov.

[3] Technical Staff Member in Nuclear Engineering and Nonproliferation Division (NEN-DO). Mailing: Los Alamos National Laboratory, PO Box 1663, MS F650, Los Alamos, New Mexico 87545. Phone: 505-665-0053. Email: cu@lanl.gov.

Table of Contents

List of Figures

List of Tables

1 Introduction

In the absence of a well-accepted, mathematical description of how units of material respond to one or more external actions (*e.g.* temperature fluctuations), scientists must often rely upon empirically-derived models (*e.g.* polynomials) to make predictions. These predictions may be **inter**polatory or **extra**polatory in nature, but irrespective of this, the predictions derive from a model that employs little-to-no physics: a potentially dangerous situation if the phenomena being modeled are, in reality, complex processes. This situation can be especially disconcerting when limited data sets are available for development of the model or when the model does not generalize well to data sets that become available after its development.

Given our increased reliance on modeling and simulation to make predictions (both interpolatory and extrapolatory) in the absence of experimental data, it befits the scientific community to explore and report upon uncertainty quantification techniques applied to previously adopted (or at least well-accepted) empirical models that derive from, or pertain to, substantial experimental data sets. Such studies, while more applied in nature, provide guidance for conducting studies on codes that are still under development. This report represents a collection of three methodologies aimed at assessing the predictive capability of the empirically-derived thermal conductivity model adopted by the nuclear fuel performance code, FRAPCON-3.4 (referred to as the "FRAPCON model"). The three methodologies adopt an optimization-based, a Bayesian inference based, and an info-gap decision theory based approach, respectively. Each considers the effect of parametric uncertainty on the ability of the model to predict uranium dioxide (UO2) thermal conductivity data from open literature sources. Following is an overview of the historical development of the FRAPCON model that is being considered in this report.

1.1 FRAPCON-3.4 Thermal Conductivity Model

The ceramic nuclear fuel, UO2, used in light water reactors is known to be a very poor semiconductor. The heat generated by fission is transferred by thermal conduction primarily by way of lattice vibrations. The dependency of the thermal diffusivity (or thermal conductivity, that is the inverse of thermal diffusivity) on temperature is traditionally expressed as

$$K_{95} = \frac{1}{A + BT}. \tag{1}$$

In this equation, A represents the effect of phonon-impurity scattering processes, and B represents the effect of phonon-phonon scattering processes [1]. This simple dependency worked well for the thermal conductivity estimation of fresh fuels, as well as of irradiated fuels. There are various excellent papers on the development of an appropriate thermal conductivity model for UO2. For example, Ronchi et al. modify Equation (1) based on new measurements, to account for ambipolar and radiation contributions to thermal conductivity. The radiation contribution was found to be small relative to the lattice vibration and ambipolar contributions. As a result, nuclear fuel performance codes like FRAPCON include a thermal conductivity

model of the following form:

$$K_{95} = \frac{1}{A + BT} + \frac{E}{T^2}\exp\left(-\frac{F}{T}\right), \tag{2}$$

where $A = 0.0452$, $B = 0.000246$, $E = 3.5E9$, and $F = 16361$. Note that the ambipolar contribution is accounted for by the right-most term and becomes important at temperatures above 1900K. Figure 1 presents the available experimental thermal conductivity data associated with fresh fuel samples (see Appendix A), along with the nominal FRAPCON thermal conductivity model given by Equation (2). It is this model that will be considered in the context of predicting thermal conductivity for fresh fuel samples.

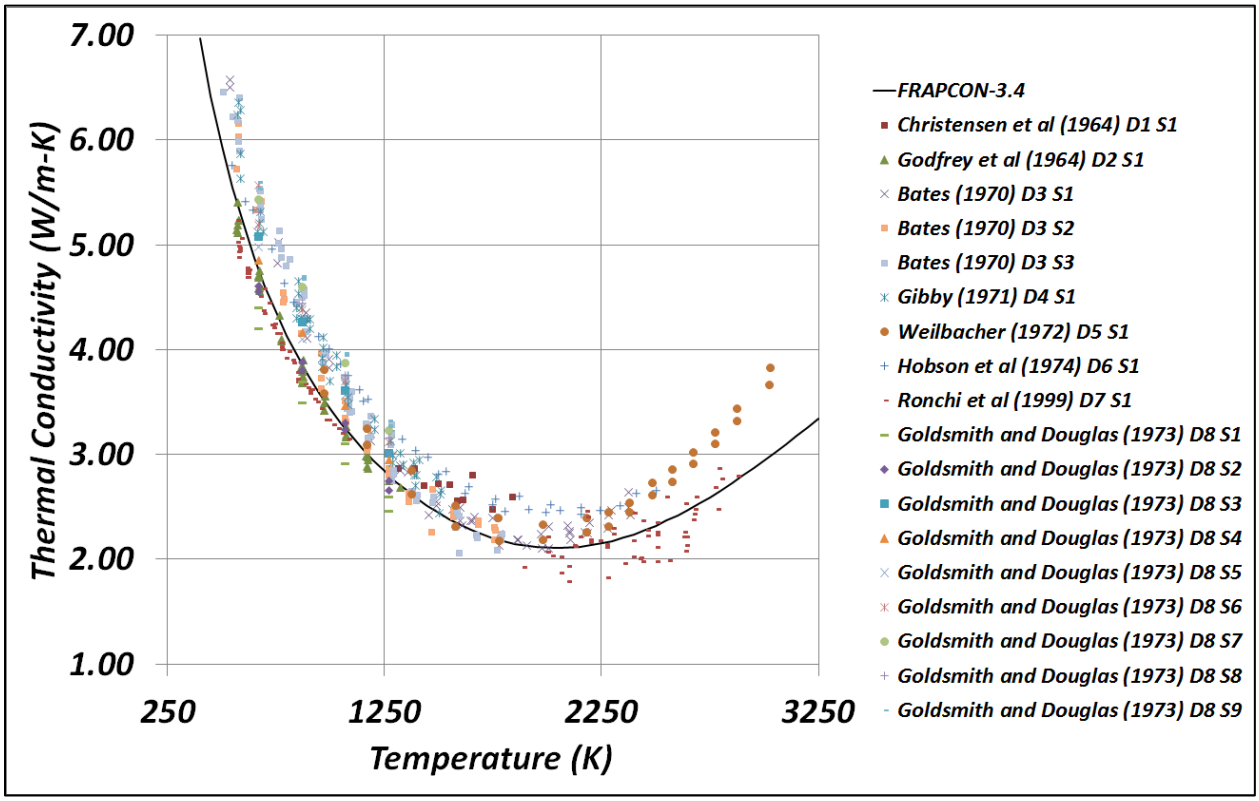

Figure 1: Experimental temperature vs. thermal conductivity plots for fresh fuel samples, with nominal FRAPCON model, as given by Equation (2)

Several authors have conducted reviews of UO2 thermal conductivity models (see *e.g.* [2,3]). These papers consider various data sets and subsequently suggest coefficients that are not necessary consistent (from reference to reference). With new measurements available, these parameters change on almost a yearly basis. For example, FRAPCON-3 and FRAPCON-3.4 implement completely different thermal conductivity models.

Regardless, the measurement of thermal conductivity of UO2 is not straightforward, and *in situ*

measurements during irradiation are not available. Typically, these measurements begin by irradiating the fuel at certain irradiation temperatures that may vary in a nuclear core, depending upon the location. The fuel is then cooled and small samples are analyzed in the laboratory by heating the sample to a desired temperature. Note that this measurement process also introduces annealing effects above certain temperatures. Furthermore, the fission process constantly produces defects that effect the correctness of A and B. These findings led Ronchi et al. to suggest an alternative model for the lattice contribution [1]:

$$K_{95} = \frac{1}{A(T_{\text{irr}}, T_{\text{ann}}, Bu) + B(T_{\text{irr}}, T_{\text{ann}}, Bu)T}, \tag{3}$$

where A and B are now *functions*, and T_{irr}, T_{ann}, and Bu are the irradiation temperature, annealing temperature, and burnup (as a percentage), respectively. FRAPCON-3 used a thermal conductivity model suggested by the Lucuta et al. [3]. FRAPCON-3.4, on the other hand, claims that the thermal conductivity model is based on the expression developed by Ohira and Itagaki [4] for the Nuclear Fuels Industries. This is given as

$$K_{95} = \frac{1}{A + BT + f(Bu) + g(Bu)h(T)} + CT^2 + DT^4, \tag{4}$$

where

$$f(Bu) = 0.00187Bu \tag{5}$$

accounts for the effect of soluble fission products,

$$g(Bu) = 0.038Bu^{0.28} \tag{6}$$

accounts for the effect of irradiation defects,

$$h(T) = \frac{1}{1 + 396\exp(-Q/T)}, \tag{7}$$

accounts for the effect of recovery of irradiation defects, and $Q = 6380$. Note that the electronic contribution (*i.e.* the ambipolar effects) is formulated differently in this model than in Equation (2). The actual thermal conductivity model implemented in FRAPCON-3.4 is given as

$$K_{95} = \frac{1}{A + BT + f(Bu) + \big(1 - 0.9\exp(-0.04Bu)\big)g(Bu)h(T)} + \frac{E}{T^2}\exp\left(-\frac{F}{T}\right). \tag{8}$$

While $f(Bu)$, $g(Bu)$, and $h(T)$ are retained from Equation (4), a new term $\big(1 - 0.9\exp(-0.04Bu)\big)$ is introduced in FRAPCON-3.4. There is no good physics argument provided in the FRAPCON manual as to why this new term is introduced. Furthermore, this

model also drops the form of the electronic contribution suggested by Ohira and Itagaki [4] and instead adapts the form suggested by Lucuta et al. [3], Fink [2], and Ronchi et al. [1]. Figure 2 presents the available experimental thermal conductivity data[4] associated with irradiated fuel samples (see Appendix B), along with the nominal FRAPCON thermal conductivity model given by Equation (8). It is this model that will be considered in the context of predicting thermal conductivity for irradiated fuel samples.

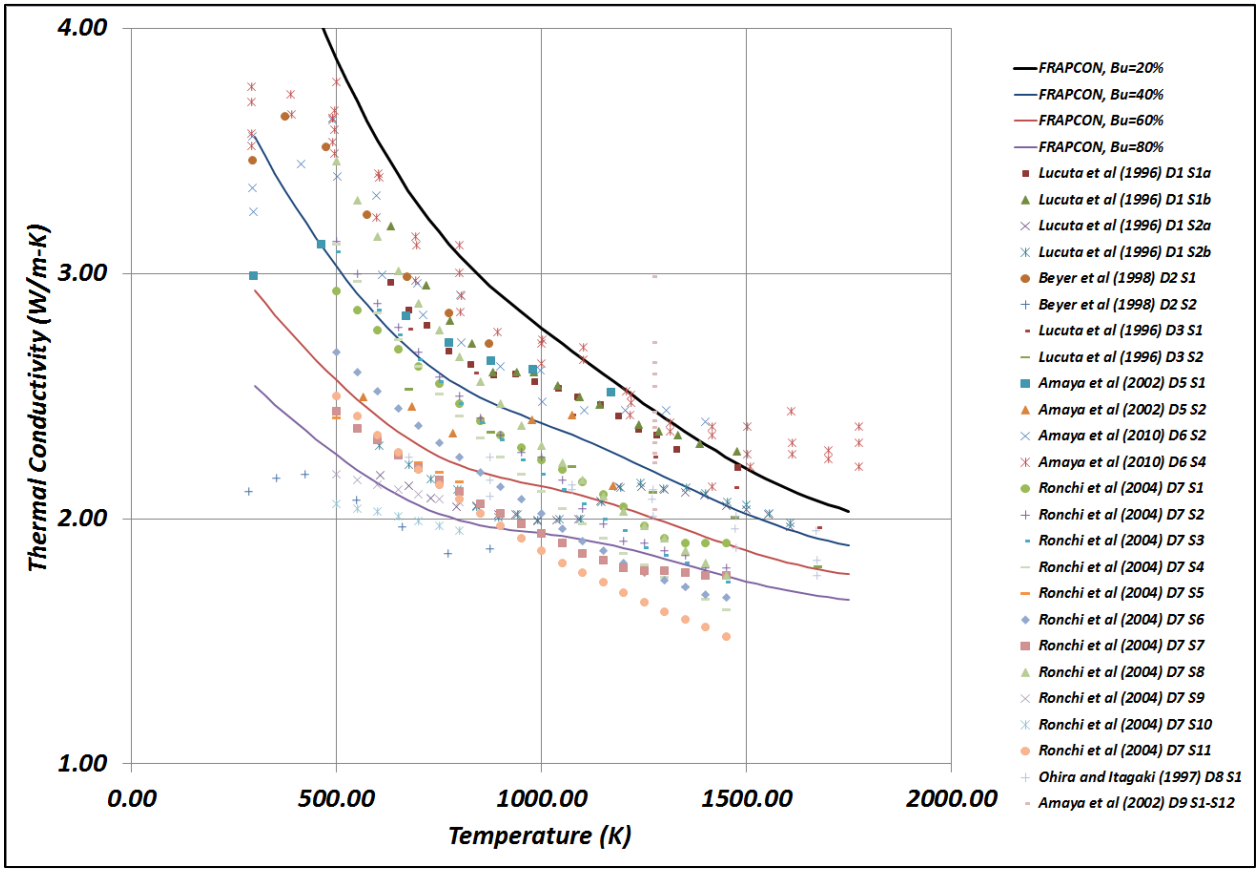

Figure 2: Experimental temperature vs. thermal conductivity plots for irradiated fuel samples, with nominal FRAPCON model, as given by Equation (8)

There is no a good explanation in the Ohira and Itakagi's paper why the functions f, g, and h should be in the form of $f + gh$. Their dependency on the coefficients A and B and their potential correlations are also not known. Table 1 presents the coefficients of A, B, E, and F recommended by different authors, indicating a large degree of variation.

[4] The data sets labeled "Amaya et al (2002) D5 S1," "Amaya et al (2002) D5 S2", "Amaya et al (2010) D6 S2," and "Amaya et al (2010) D6 S4" in Figure 2 are not included in the proceeding analyses due to inconsistencies identified by the authors.

Table 1: Values of thermal conductivity model parameters from different references

Parameter Name	FRAPCON -3	FRAPCON -3.4	Ohira and Itagaki	Lucuta et al.	Ronchi et al.	Fink
A (m-K/W)	0.0375	0.0452	0.0452	0.0375	0.06548	0.075408
B (m-K/W/K)	2.165E-4	2.46E-4	2.46E-4	2.165E-4	0.23533	0.17692
E (W-K/m)	4.715E9	3.5E9	-	4.715E9	6400*	6400*
F (K)	16361	16361	-	16361	16.35	16.35
C (W/m-K/K^2)	-	-	-5.47E-9	-	-	-
D (W/m-K/K^4)	-	-	2.29E-14	-	-	-

*divided by $T^{5/2}$ not T^2

The fuel companies may also have different coefficients specific to their fuels. It is expected that the coefficients A, B, E, and F are calibrated from fresh fuel data first and irradiation effects are introduced by examining trends in the irradiated data. In this research, the authors collected as much data from open literature as could be found, in order to assess the model parameters, independent of model developers. The authors assert that the irradiation effects should be included in the lattice term as suggested by [1]. Instead, previous authors have introduced additive terms in the denominator of the thermal conductivity equation.

1.2 Report Organization

In this research, the authors consider the thermal conductivity models in FRAPCON-3.4 (*i.e.* Equations (2) and (8) for the fresh and irradiated fuel samples, respectively) and attempt to understand the correlation issues between A and B from Equation (2) and f, g, h, and the extra term from Equation (8). Section 2 presents the results obtained from optimizing the parameters of the FRAPCON model using a genetic algorithm, where valuable insight is gained to inform the assessments in Sections 3 and 4. These latter sections will focus more on UQ, approaching the problem from two distinct viewpoints. Section 3 adopts a Bayesian probabilistic approach, presenting the results of a series of Markov Chain Monte Carlo executions that yield posterior probability density functions of the uncertain parameters, conditioned on the available data. Section 4 employs a non-probabilistic approach, namely info-gap decision theory, to assess the "robustness" of the FRAPCON model, when the uncertain parameters are considered to be truly unknown quantities, centered about their nominal values.

Following the presentation of results for the FRAPCON model, Section 5 of this report outlines a plan to conduct a similar study on *Idaho National Laboratory's* (INL) nuclear fuel performance code, BISON [5], developed under INL's *Multiphysics Object Oriented Simulation Environment* (MOOSE) [6]. In particular, the models that make use of empirically-derived coefficients to fit experimental data will be considered.

2 Genetic Algorithm Optimization Analyses

This section reports upon the results of an effort at optimizing the uncertain parameters of the FRAPCON model that aims to minimize the root mean square difference between the code predictions and the experimental data. While the authors admit that this effort does little to quantify parametric uncertainty associated with the FRAPCON model, it does represent a state-of-the-practice approach to model calibration, in that many such efforts simply rely on optimizing a set of model parameters (both physics- and empirically-based) to "best-fit" one or more data sets. The authors contend that such "blind" optimizations of model parameters can lead to false confidence in the predictive capability of the model (*i.e.* "I optimized the model parameters to reduce model error, so my new, optimized model must be more predictive."). The authors' concern is especially relevant when dealing with empirically-derived models, in that little-to-no intuition can be derived from such models. While qualitative and quantitative mechanisms have been proposed [7,8,9] to highlight the effects (on predictive capability) of this and other, similar concerns, it is nonetheless commonplace to see optimization as the *de facto* treatment for model calibration. This is not to say that optimization procedures do not have a place in model calibration, but rather that reliance on optimization alone results in an incomplete picture of the problem at best.

2.1 Problem Formulation

Formally, the optimization problem may be stated as

$$J(\boldsymbol{\theta}) = \min_{\boldsymbol{\theta}} E_{\mathrm{RMS}}(\boldsymbol{\theta}), \tag{9}$$

where

$$E_{\mathrm{RMS}}(\boldsymbol{\theta}) = \sum_{i=1}^{n} \left(\frac{1}{m_n} \sum_{j=1}^{m_n} \left(K_{i,j}^{\mathrm{exp}} - K_{i,j}^{\mathrm{mod}}(\boldsymbol{\theta}) \right)^2 \right)^{1/2}. \tag{10}$$

In Equation (10), n is the number of data sets, m_n is the number of data points in the n^{th} data set, K is the thermal conductivity of the fuel, and the superscripts "exp" and "mod" denote experimental data and model predictions, respectively.

The authors adopted a *Genetic Algorithm* (GA) to solve the optimization problem defined by Equation (9). GAs are well-accepted in the numerical optimization literature for their ability to traverse local optima while searching for a global optimum [10]. GAs model the optimization problem as an evolutionary or "survival of the fittest" process, where "fitness" of an "individual" is measured by way of an objective function (*e.g.* Equation (10)). Individuals comprise a number of "genes" that represent the parameters over which the optimization is being considered; for the implementation discussed herein, the genes are simply

the uncertain model parameters discussed in Section 1.1. More condensed representations (*e.g.* principal components) can also be employed.

Algorithmically, GAs begin by initiating a population of individuals, often random in nature. Each individual is evaluated for its fitness and ranked from highest to lowest, where the most fit individual(s) is carried over to the next generation (*i.e.* "elitism"). The "parent" individuals then undergo "selection" and "crossover" whereby individuals are first paired up and then swap genes with some fixed rate of success. The result is a new, "child" population of individuals. Note that the selection process does not mandate that only the most fit individuals undergo crossover (*i.e.* relatively fit and relatively unfit individuals can swap genes). The intent of the selection and crossover processes is to promote diversity in the population, while ultimately aiming to combine the most attractive features from two parent individuals into a new, child individual. Following crossover, the child individuals undergo "mutation" whereby a small number of genes are randomly perturbed, the aim of which is to prevent individuals from becoming "trapped" in local minima. Following mutation, the process repeats, where the child individuals become parent individuals, and so on.

Particular to this report, the authors employed the GA implementation provided by the Global Optimization Toolbox in MATLAB™ [11]. The pertinent functions adopted for the analyses discussed in Section 2.2 are stochastic universal sampling (or stochastic uniform) selection, single-point crossover, and Gaussian mutation, respectively. Stochastic uniform selection is a fitness-proportional selection function that is similar to roulette wheel selection [10], except that the wheel is spun *once* and the algorithm moves along the wheel in equal-sized steps to select parents. This eliminates the potential (although unlikely) problem encountered with the basic roulette wheel selection, in that a series of particularly "unlucky" spins of the roulette wheel will land only on low fitness individuals (becoming low fitness parent individuals). For single-point crossover, the algorithm simply chooses a gene index, and swaps the genes above *or* below that gene index. Lastly, the Gaussian mutation function adopts a scaled Gaussian function to perturb a gene from its nominal value (*i.e.* that resulting from crossover). MATLAB™ also adopts a scaling factor that reduces the frequency of mutation as the number of generations increase. More details about the MATLAB™ GA and the available functions can be found in [11]. Following in Section 2.2 is a presentation and discussion of the results obtained from executions of the GA described previously.

2.2 Results

The results presented in this section are organized around two sub-sections that pertain to two combinations of data sets and model parameters. Section 2.2.1 pertains to thermal conductivity data associated with fresh fuel samples, which is analyzed using the FRAPCON-3.4 thermal conductivity model given by Equation (2). Section 2.2.2 then pertains to thermal conductivity data associated with irradiated fuel samples, which is analyzed using the FRAPCON-3.4 thermal conductivity model given by Equation (8).

2.2.1 Data / Model for Fresh Fuel Samples

This section begins by presenting Figure 3: a comparison between the experimental data and the model predictions from the thermal conductivity nominal, given in Equation (2). It can be seen in Figure 3 that for the most part, the nominal model predictions are reasonably close to the experimental data or, in the least, follow a trend that parallels the 45° line (solid, black line). Applying the GA optimization procedure outlined previously, allowing 50 percent deviation from the nominal parameter values, yields a very similar comparison plot, as given by Figure 4.

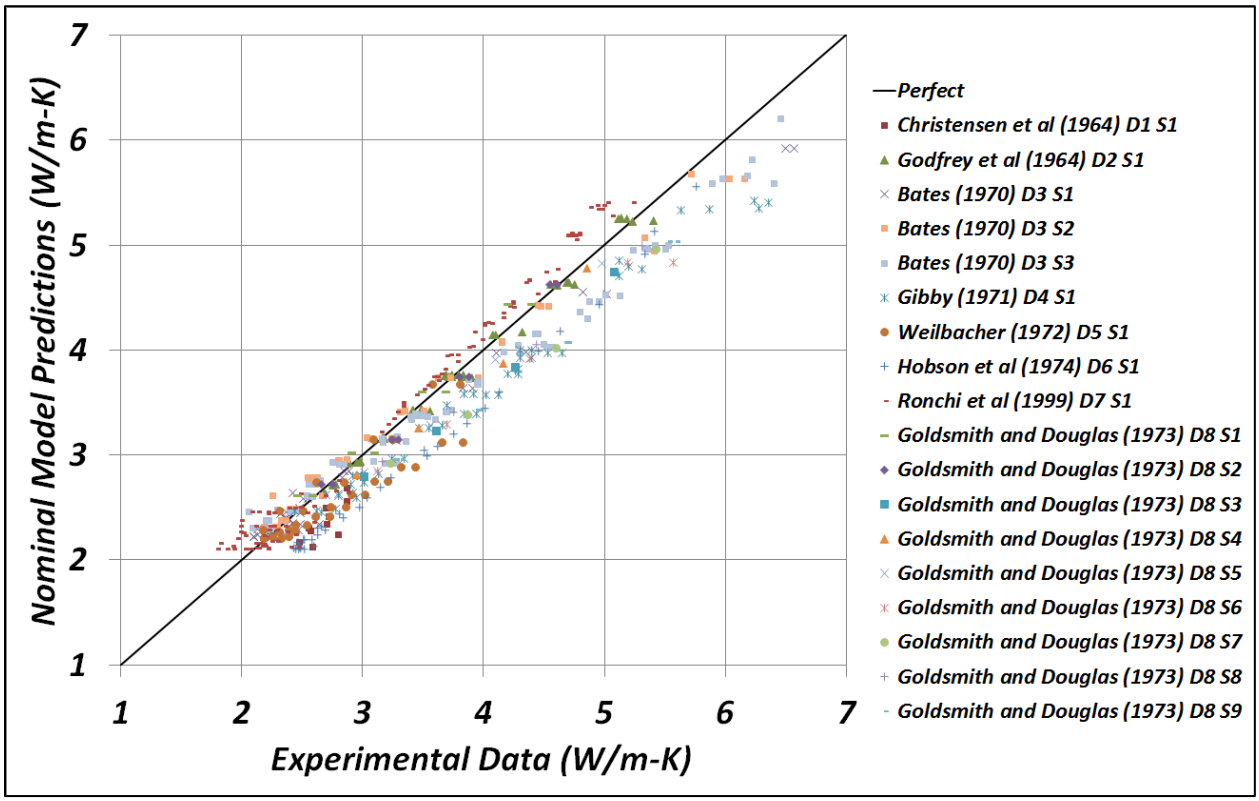

Figure 3: Comparison between experimental data and **nominal** model predictions for thermal conductivity

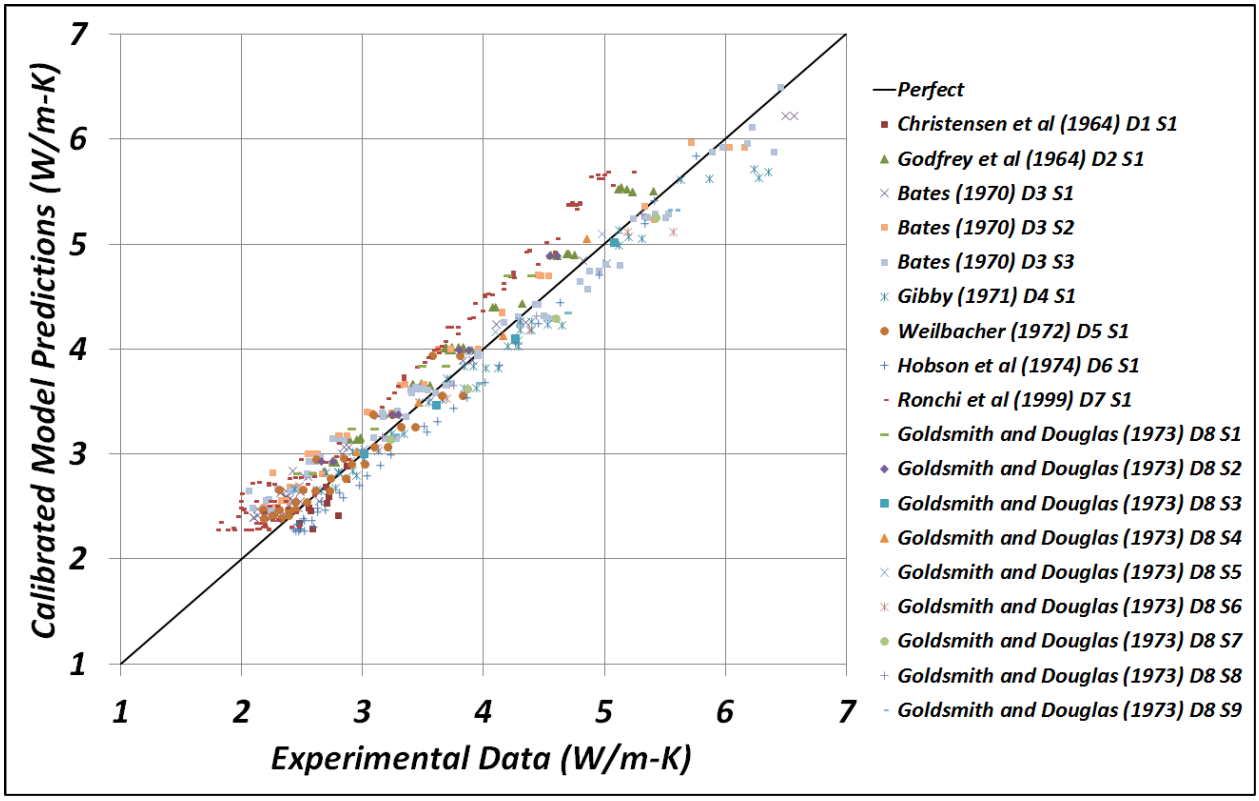

Figure 4: Comparison between experimental data and **GA-optimized** model predictions for thermal conductivity, allowing **50%** deviation from the nominal parameter values

The primary difference between Figure 3 and Figure 4 is that the model predictions generally shift upward, yielding predictions that more closely aligned with the experimental data, in the range from 3.0 to 7.0. A more quantitative explanation of these results is given in Table 2 and Table 3, where Table 2 presents the nominal parameter values and the GA-optimized parameter values (with relative differences, in percent) and Table 3 presents the values of the objective function (Equation (10)) for the nominal case and the GA-optimizations.

The primary result of interest from Table 2 lies in disparity between the optimized values of the third (E) and fourth (F) parameters. Whereas the third parameter varies by 50 percent (*i.e.* the upper bound permitted by the GA optimization), the fourth parameter only varies by less than 5%. The fact that these parameters are effectively at odds with each other (see Equation (2)) is the likely cause of this result, where it seems that the exponential dominates the behavior of the second term, but an alternative, sensitivity-based assessment is that the model is insensitive to the third parameter and very sensitive to the fourth parameter. This issue will be discussed further, in the context of info-gap robustness in Section 4.2.1.

Moving on to Table 3, it is seen that the GA optimization reduces the value of the objective function by approximately 26%, as compared with that of the nominal model. However, it is also seen that when the allowable deviation from the nominal parameter values is reduced to ten

percent, the reduction in the objective function is *nearly the same*. While this may not be an entirely intuitive result, the GA-optimized parameter values given in Table 4 shed light on this result, in that the values of the first (A) and second (B) parameters are effectively the same (*i.e.* increasing and decreasing by approximately 8.5 percent, respectively), regardless of the allowable deviation. This implies that the primary mechanism by which the optimization is achieved is by way of varying the first and second parameters. This, together with the earlier observation that "model predictions generally shift upward … in the range from 3.0 to 7.0" is consistent however, in that the first two parameters offer the primary mechanism by which low-temperature / high-conductivity predictions are made (*i.e.* ambipolar contributions, represented by the right-most term of Equation (2), are insignificant at temperatures below 1900K).

Table 2: GA-optimized parameter values, allowing **50%** deviation from the nominal parameter values

Parameter Name	Nominal Value	GA-Optimized Value	Relative Difference (%)
A (m-K/W)	0.0452	0.04911	8.7%
B (m-K/W/K)	0.000246	0.0002230	9.3%
E (W-K/m)	**3.50E+09**	**5.250E+09**	**50.0%**
F (K)	16361	17101.6	4.5%

Table 3: Objective function evaluations associated with GA-optimized parameter values (fresh fuel parameters / data only)

Analysis	$E_{\mathrm{RMS}}(\boldsymbol{\theta})$	Relative Improvement (%)
Nominal	5.22	-
GA-Opt (50%)	3.84	26.4%
GA-Opt (10%)	**3.86**	**26.1%**

Table 4: GA-optimized parameter values, allowing **10%** deviation from the nominal parameter values

Parameter Name	Nominal Value	GA-Optimized Value	Relative Difference (%)
A (m-K/W)	0.0452	0.04889	8.2%
B (m-K/W/K)	0.000246	0.0002240	8.9%
E (W-K/m)	**3.50E+09**	**3.850E+09**	**10.0%**
F (K)	16361	16296.4	0.4%

2.2.2 Data / Model for Irradiated Fuel Samples

As in the previous case, this section begins by presenting a comparison between the experimental data and the model predictions from the thermal conductivity nominal, given in Equation (8). In contrast to the previous section, however, is the fact that there is no consistent trend in the

relationship between the experimental data and the nominal model predictions. This issue is not resolved by the GA optimization, the analogous plot for which is presented in Figure 6. This is a rather unexpected and obviously disconcerting result, especially given the recent (*i.e.* 2010) adoption of this model for predicting the behavior of irradiated fuel samples.

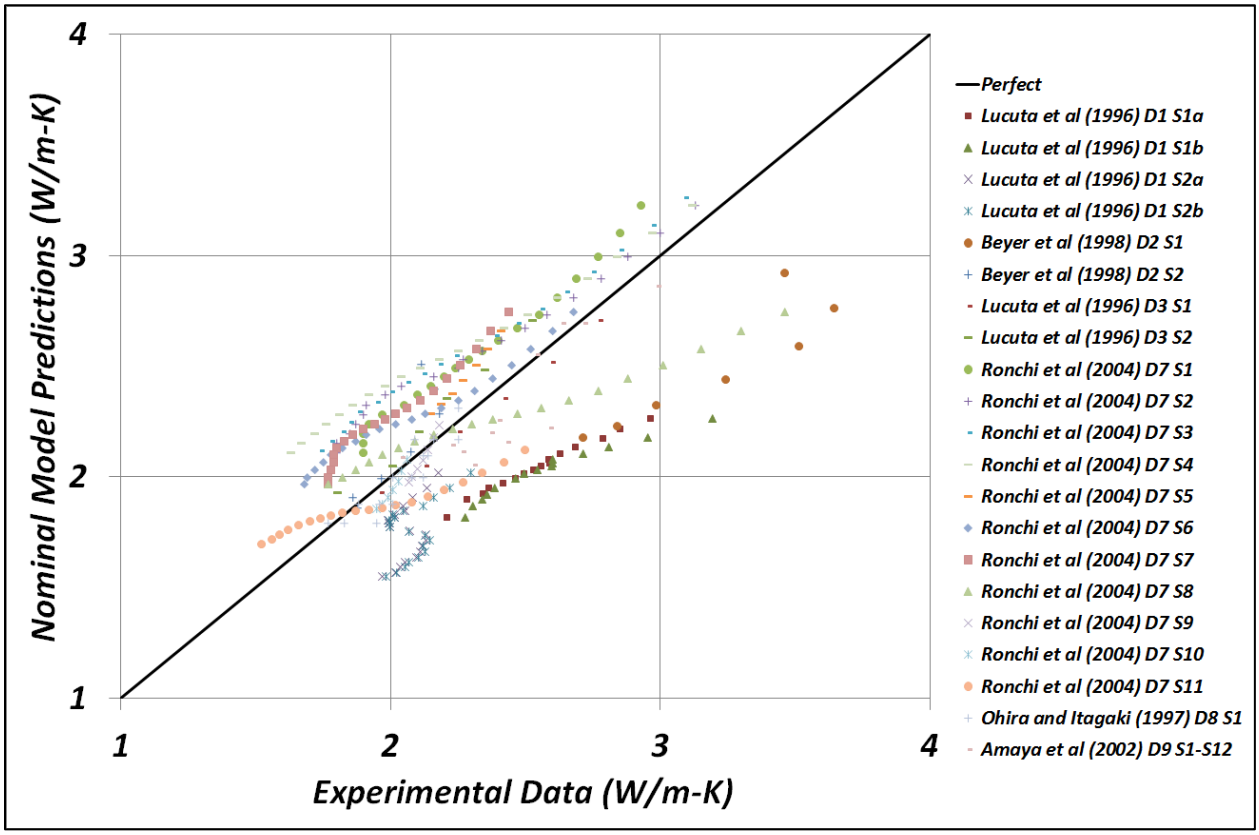

Figure 5: Comparison between experimental data and **nominal** model predictions for thermal conductivity

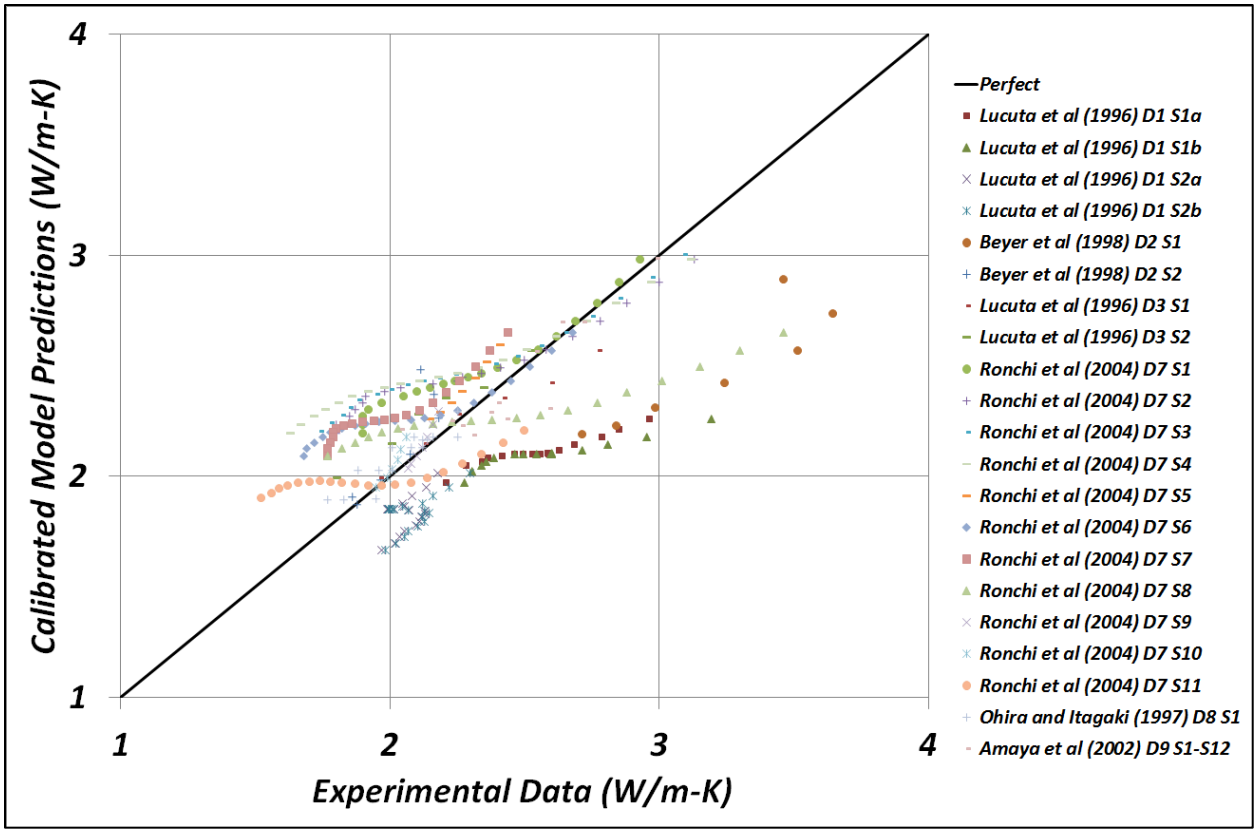

Figure 6: Comparison between experimental data and **GA-optimized** model predictions for thermal conductivity, allowing **50%** deviation from the nominal parameter values

Upon examination of Table 5, the outlook does not improve, as seven of the eleven parameters assume "optimal" values at either the lower or upper bound; an eighth $(g(Bu)_{\mathrm{A}})$ parameter assumes a value that deviates by 31.5 percent. Perhaps adopting an alternative objective function may be in order, but the fact that a majority of the parameters deviate significantly from their nominal values does little to engender confidence as to the predictive capability of the model. For completeness, Table 6 provides the values of the objective function for the nominal and two GA optimizations, for allowable deviations of 50 percent and ten percent.

Table 5: GA-optimized parameter values, allowing **50%** deviation from the nominal parameter values

Parameter Name	**Nominal Value**	**GA-Optimized Value**	**Relative Difference (%)**
A (m-K/W)	0.0452	0.03096	31.5%
B (m-K/W/K)	0.000246	0.0002450	0.4%
E (W-K/m)	3.50E+09	1.750E+09	50.0%
F (K)	16361	24541.5	50.0%
f(Bu)	0.00187	0.000935	50.0%
0.9 Factor	0.9	0.450	50.0%
0.04 Factor	0.04	0.060	50.0%
$g(Bu)_A$	0.038	0.0570	50.0%
$g(Bu)_B$	0.28	0.2925	4.5%
h(T)	396	198.0	50.0%
Q	6380	6077.2	4.7%

Table 6: Objective function evaluations associated with GA-optimized parameter values (irradiated fuel parameters / data only)

Analysis	$\boldsymbol{E_{\mathrm{RMS}}(\theta)}$	**Relative Improvement (%)**
Nominal	7.19	-
GA-Opt (50%)	6.40	11.0%
GA-Opt (10%)	6.78	5.7%

To connect this with the previous section, the authors employed the first four parameters presented in Table 5 to make predictions of the thermal conductivities associated with the *fresh* fuel samples. If the model represented by Equation (8), calibrated using the irradiated data only, is consistent with the underlying physics exhibited by the fresh *and* irradiated fuel samples, the predictions should be reasonably accurate. Table 7 indicates that this is not the case, as the predictions are actually *worse* than those associated with the *nominal* FRAPCON model. Clearly, calibration to the data associated with the irradiated fuel samples only is insufficient for the purposes of improving the model's predictive capability.

Table 7: Objective function evaluations associated with GA-optimized parameter values (fresh fuel parameters, irradiated data)

Analysis	$\boldsymbol{E_{\mathrm{RMS}}(\theta)}$	**Relative Improvement (%)**
Nominal	5.22	-
GA-Opt (50%)	5.57	-6.7%

To explore this issue further, a third analysis is conducted using the data associated with the irradiated fuel samples, whereby the first four parameters are held fixed at the values given in Table 4, and the remaining seven parameters are allowed to vary. Table 8 presents the values of the objective function associated with this analysis. The results indicate that fixing the fresh fuel parameters at their previously GA-optimized values still permits improvement over the nominal model. This goes back to an earlier statement in Section 1.1 stating that the first four parameters of Equation (8) "are calibrated from fresh fuel data first and irradiation effects are introduced by examining trends in the irradiated data." That said, the authors are led to question whether the mathematical form of Equation (8) is valid for predicting thermal conductivities associated with irradiated fuel samples. This question will be further explored in the subsequent sections.

Table 8: Objective function evaluations associated with GA-optimized parameter values (irradiated fuel parameters / data only with fresh fuel parameters held fixed at the values given in Table 4)

Analysis	$\boldsymbol{E_{\mathrm{RMS}}(\theta)}$	**Relative Improvement (%)**
Nominal	7.19	-
GA-Opt (50%)	6.60	8.2%
GA-Opt (10%)	7.16	< 1%

3 Markov Chain Monte Carlo Analyses

In parametric Bayesian analysis, observed data $\boldsymbol{y}$ are sampled from a distribution $g(\boldsymbol{y}|\boldsymbol{\theta})$, where g is a specified family of distributions (*e.g.* Gaussian) and $\boldsymbol{\theta}$ is a collection of parameters having unknown values. The family of distributions g is often determined by the nature of experimental errors. For example, a particular fuel conductivity dataset could be modeled as follows,

$$\boldsymbol{y} = \boldsymbol{\eta}(\boldsymbol{\theta}) + \boldsymbol{\varepsilon} \tag{11}$$

where $\boldsymbol{\eta}(\boldsymbol{\theta})$ is the vector of conductivity model outputs evaluated at model parameters $\boldsymbol{\theta}$ and corresponding to the conditions producing $\boldsymbol{y}$, and $\boldsymbol{\varepsilon}$ is the vector of observational errors. These errors are often assumed to be independent, zero-mean, Gaussian with specified standard deviations. In this scenario, pursued in the subsequent analyses, the family g is multivariate Gaussian having mean $\boldsymbol{\eta}(\boldsymbol{\theta})$ and specified standard deviations.

In the following discussion, the sampling distribution g viewed as a function of unknown parameters $\boldsymbol{\theta}$ (for given data values $\boldsymbol{y}$) will be referred to as the *likelihood function*, $L(\boldsymbol{\theta}|\boldsymbol{y}) \equiv g(\boldsymbol{y}|\boldsymbol{\theta})$. For varying $\boldsymbol{\theta}$, higher likelihood values indicate parameter settings for which the conductivity model output exhibits greater consistency with the observed conductivity data $\boldsymbol{y}$. To complete the Bayesian framework, initial (prior) uncertainty in the values of $\boldsymbol{\theta}$ is represented by a distribution π, referred to as the *prior distribution*. In the subsequent analyses, π is assumed to be a Uniform distribution on pre-specified ranges for each model parameter presented in Equations (2) and (8). Given observed conductivity data $\boldsymbol{y}$, inference about $\boldsymbol{\theta}$ is based entirely on the *posterior distribution*, given by

$$\pi(\boldsymbol{\theta}|\boldsymbol{y}) = \frac{L(\boldsymbol{\theta}|\boldsymbol{y})\boldsymbol{\pi}(\boldsymbol{\theta})}{\int L(\boldsymbol{\theta}|\boldsymbol{y})\boldsymbol{\pi}(\boldsymbol{\theta})d\boldsymbol{\theta}}. \tag{12}$$

In words, the posterior distribution utilizes the conductivity data $\boldsymbol{y}$ to update the prior uncertainty about $\boldsymbol{\theta}$, resulting in new uncertainty quantification for $\boldsymbol{\theta}$ that incorporates information from both prior knowledge π and observational data $\boldsymbol{y}$.

In the analyses of this section, the posterior normalizing constant $\int L(\boldsymbol{\theta}|\boldsymbol{y})\boldsymbol{\pi}(\boldsymbol{\theta})d\boldsymbol{\theta}$ is not computable in closed form, as the conductivity models are non-linear. Therefore, exact posterior calculations are not possible. Fortunately, technology exists for generating samples $\boldsymbol{\theta}_i$ from the posterior distribution $\pi(\boldsymbol{\theta}|\boldsymbol{y})$. The methodology we employ is referred to as *Markov Chain Monte Carlo* (MCMC) sampling, which involves establishing the target distribution $\pi(\boldsymbol{\theta}|\boldsymbol{y})$ as the stationary distribution of a Markov Chain. The following sampling algorithm used in the subsequent analyses is one of many possibilities that accomplishes this goal:

1. Set the iteration counter $i = 1$ and select a starting value for $\boldsymbol{\theta}$, denoted $\boldsymbol{\theta}^{(0)}$.

2. Suppose $\boldsymbol{\theta}$ has m elements, of which the first $(j-1)$ have already been updated. The j^{th} parameter is updated as follows. Let $\boldsymbol{\theta}_c = \left(\theta_1^{(i)}, \ldots, \theta_{j-1}^{(i)}, \theta_j^{(i-1)}, \theta_{j+1}^{(i-1)}, \ldots, \theta_m^{(i-1)}\right)$ be the current value of $\boldsymbol{\theta}$, and propose a new value for θ_j (denoted θ_j^*) by sampling from the specified distribution $q_j\left(\theta \middle| \theta_j^{(i-1)}\right)$. Taking, $\boldsymbol{\theta}_* = \left(\theta_1^{(i)}, \ldots, \theta_{j-1}^{(i)}, \theta_j^*, \theta_{j+1}^{(i-1)}, \ldots, \theta_m^{(i-1)}\right)$ we set $\theta_j^{(i)} = \theta_j^*$ with probability
$$\min\left\{1, \frac{L(\boldsymbol{\theta}_*|\boldsymbol{y})\boldsymbol{\pi}(\boldsymbol{\theta}_*)q_j(\boldsymbol{\theta}_c|\boldsymbol{\theta}_*)}{L(\boldsymbol{\theta}_c|\boldsymbol{y})\boldsymbol{\pi}(\boldsymbol{\theta}_c)q_j(\boldsymbol{\theta}_*|\boldsymbol{\theta}_c)}\right\};$$
otherwise set $\theta_j^{(i)} = \theta_j^{(i-1)}$. Once the m^{th} parameter has been updated in this fashion, the i^{th} iteration has been completed and we denote the resulting sample by $\boldsymbol{\theta}_i$.
3. Repeat the previous step n times, resulting in n samples $\boldsymbol{\theta}_1, \ldots, \boldsymbol{\theta}_n$.

An initial subset of iterations $\boldsymbol{\theta}_i$ are discarded as burn-in samples, as these iterations are required for the Markov chain to 'forget' its starting value $\boldsymbol{\theta}^{(0)}$ and converge to its stationary distribution (*i.e.* the posterior). It is desirable to choose a $\boldsymbol{\theta}^{(0)}$ having reasonably high posterior probability. In our analyses, we set $\boldsymbol{\theta}^{(0)}$ to the nominal values of the model parameters (see Equations (2) and (8)). The proposal distribution $q_j(\theta|\theta_c)$ is taken to be Uniform on the interval $\left(\theta_c - s_j/2\,, \theta_c + s_j/2\right)$. The interval width s_j is chosen adaptively during the burn-in period of the MCMC algorithm. Specifically, the algorithm of [12] is used: a specified nominal value of s_j is expanded and contracted dyadically by a specified number of levels. During burn-in, the algorithm repeatedly cycles through each resulting level, collecting acceptance statistics. At the conclusion of burn-in, the acceptance statistics are used to fit a logistic regression model of acceptance probability versus interval width. The interval width s_j is estimated by choosing the value corresponding to a targeted acceptance rate, approximately 40% in the subsequent analyses. The estimated interval widths for each parameter are then used in the above MCMC algorithm post burn-in to generate samples of $\boldsymbol{\theta}$ from the posterior distribution $\pi(\boldsymbol{\theta}|\boldsymbol{y})$. For post-burn-in samples $\boldsymbol{\theta}_{b+1}, \ldots, \boldsymbol{\theta}_n$, posterior conductivity model predictions for any specified fuel conditions are obtained by computing $\boldsymbol{\eta}(\boldsymbol{\theta}_{b+1}), \ldots, \boldsymbol{\eta}(\boldsymbol{\theta}_n)$. Further information on technical and practical considerations for MCMC and its implementation can be found in [13].

Let $\boldsymbol{\theta}_f$ and $\boldsymbol{\theta}_r$ denote the parameters in the conductivity models of fresh (*i.e.* Equation (2)) and irradiated (*i.e.* Equation (8)) fuel samples, respectively. Here $\boldsymbol{\theta}_r = \left(\boldsymbol{\theta}_f, \boldsymbol{\theta}_{r-f}\right)$, where $\boldsymbol{\theta}_{r-f}$ represents parameters in the irradiated fuel conductivity model that are not in common with the fresh fuel conductivity model. Three analyses will be conducted: (a) Calibration of $\boldsymbol{\theta}_f$ to fresh fuel conductivity data only, (b) Calibration of $\boldsymbol{\theta}_r$ to irradiated fuel conductivity data only, and (c) Simultaneous calibration of $\boldsymbol{\theta}_f$ and $\boldsymbol{\theta}_{r-f}$ to fresh and irradiated fuel data. Note that (c) facilitates discovery of parameter settings $\boldsymbol{\theta}_f$ and $\boldsymbol{\theta}_{r-f}$, with uncertainty quantification, that are consistent with all available experimental data. The likelihood functions for these Analyses (a), (b) and (c) are given by Equations (13), (14), (15), respectively, as

$$L_f\left(\boldsymbol{\theta}_f \middle| \boldsymbol{y}_1^f, \ldots, \boldsymbol{y}_{n_f}^f\right) = \prod_{i=1}^{n_f} L_f\left(\boldsymbol{\theta}_f \middle| \boldsymbol{y}_i^f\right), \tag{13}$$

$$L_r\left(\boldsymbol{\theta}_r \middle| \boldsymbol{y}_1^r, \ldots, \boldsymbol{y}_{n_r}^r\right) = \prod_{i=1}^{n_r} L_r\left(\boldsymbol{\theta}_r \middle| \boldsymbol{y}_i^r\right), \tag{14}$$

$$L_{fr}\left(\boldsymbol{\theta}_f, \boldsymbol{\theta}_{r-f} \middle| \boldsymbol{y}_1^f, \ldots, \boldsymbol{y}_{n_f}^f, \boldsymbol{y}_1^r, \ldots, \boldsymbol{y}_{n_r}^r\right) = \prod_{i=1}^{n_f} L_f\left(\boldsymbol{\theta}_f \middle| \boldsymbol{y}_i^f\right) \prod_{i=1}^{n_r} L_r\left(\boldsymbol{\theta}_f, \boldsymbol{\theta}_{r-f} \middle| \boldsymbol{y}_i^r\right), \tag{15}$$

where n_f and n_r are the numbers of fresh and irradiated fuel conductivity datasets, respectively. For each dataset, we assume the specified standard deviations in the $\boldsymbol{\varepsilon}$ error model are equal to one-third of 10% of the observed data values.

3.1 Results

The results presented in this section are organized around *three* sub-sections that pertain to *three* combinations of data sets and model parameters. Section 3.1.1 pertains to thermal conductivity data associated with fresh fuel samples, which is analyzed using the FRAPCON-3.4 thermal conductivity model given by Equation (2). Section 3.1.2 then pertains to thermal conductivity data associated with irradiated fuel samples, which is analyzed using the FRAPCON-3.4 thermal conductivity model given by Equation (8). Unique to the MCMC analysis, Section 3.1.3 pertains to the thermal conductivity data associated with both the fresh and irradiated fuel samples in a single MCMC analysis, using both FRAPCON-3.4 thermal conductivity models given by Equations (2) and (8).

3.1.1 Data / Model for Fresh Fuel Samples

Table 9 presents the mean values of the parameters generated by MCMC Analysis (a), in which the data / model associated with the fresh fuel samples only are considered. The most interesting conclusion from this table is that its results are nominally very similar to those associated with the GA optimization discussed in Section 2.2.1. That is, the third parameter (E) varies considerably from the nominal value, while the remaining parameters vary by what may reasonably be considered an acceptable level (*i.e.* +/-10%). In effect, this lends credence to the discussion in Section 2.2.1, but the MCMC analysis provides considerably more information than the point estimate offered by the GA optimization. Table 10 does show that the mean values of the parameters produce an improvement in the overall predictive capability of the model (vis-à-vis a reduction in the value of the $E_{\mathrm{RMS}}(\boldsymbol{\theta})$).

Table 9: Mean parameter values from MCMC Analysis (a), allowing **50%** deviation from the nominal parameter values

Parameter Name	Nominal Value	MCMC Mean Value	Percent Difference	Standard Deviation	Percent of Mean
A (m-K/W)	0.0452	0.04696	3.9%	0.00149	3.2%
B (m-K/W/K)	0.000246	0.0002360	4.1%	0.0000016	0.7%
E (W-K/m)	3.50E+09	5.075E+09	45.0%	0.1605E+09	3.2%
F (K)	16361	17513.2	7.0%	94.7	0.5%

Table 10: Objective function evaluations associated with the mean parameter values from the MCMC analysis (fresh fuel parameters / data only)

Analysis	$E_{\mathrm{RMS}}(\boldsymbol{\theta})$	Relative Improvement (%)
Nominal	5.22	-
MCMC (50%)	4.43	15.1%

Arguably, the most attractive products of MCMC analyses that are not offered by many optimization-based analyses are the estimates of the posterior distributions associated with each parameter. For MCMC Analysis (a), the posteriors (univariate and bivariate) associated with the four parameters are presented in Figure 7, where the ordering of the parameters is left-to-right / top-to-bottom (*e.g.* posteriors associated with parameter *A* are on the first row / column, and so on).

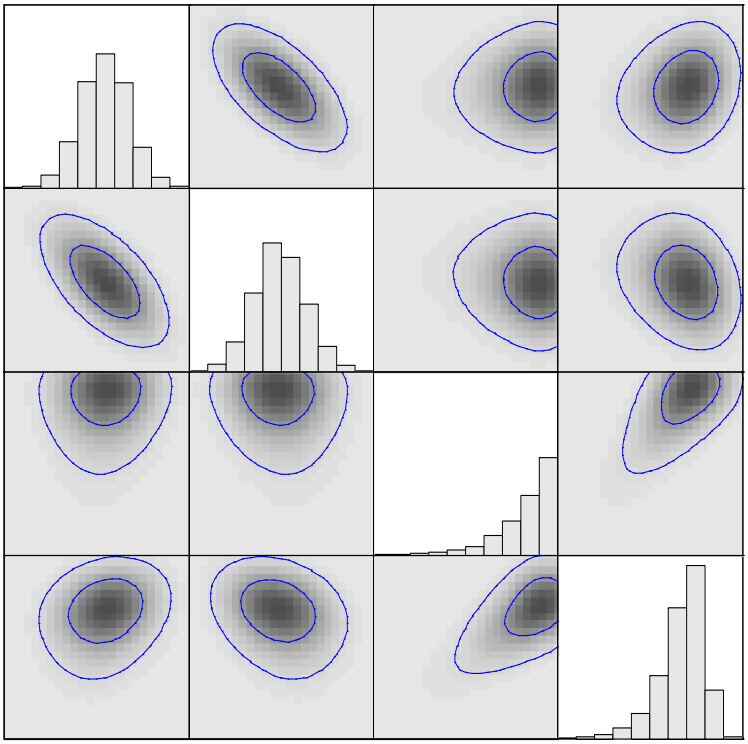

Figure 7: Estimates of univariate (diagonal) and bivariate (off-diagonal) marginal posterior distributions for MCMC Analysis (a)

There are two primary results of interest from Figure 7. The first is with regard to the third (E) parameter, in that the univariate posterior distribution indicates that a more suitable value may lie outside of the prescribed +/-50%. While this is useful information and may warrant further investigation, it will be shown in Section 4.2.1 that the third parameter is the least influential with respect to "info-gap robustness" of the FRAPCON model.

The second result of interest pertains to: the presence of a negative correlation between the first (A) and second (B) parameters and the presence of a positive correlation between the third (E) and fourth (F) parameters. The format of Equation (2) explains the presence of these relationships, but of interest is whether these relationships remain present in MCMC Analyses (b) and (c). A reasonable expectation is that the additional parameters associated with Equation (8) will reduce the influences of the first through fourth parameters on the conductivity, thereby diminishing the correlations. However, an equally reasonable expectation is that the combination of the fresh and irradiated data sets (*i.e.* MCMC Analysis (c)) will cause variances on the posteriors to reduce, possibly enhancing the correlations.

3.1.2 Data / Model for Irradiated Fuel Samples

Analogous to the GA optimization analysis discussed in Section 2.2.2, the results of Table 11 present mean values for eight of the eleven parameters that deviate from the nominal values by

more than +/-10%, with six of those deviating by more than +/-30%. More disconcerting than the results of Table 11, however, is the substantial reduction in agreement of the model with the experimental data, as presented by the *increased* value of the $E_{\mathrm{RMS}}(\boldsymbol{\theta})$ in Table 12.

Table 11: Mean parameter values from MCMC Analysis (b), allowing **50%** deviation from the nominal parameter values

Parameter Name	Nominal Value	MCMC Mean Value	Percent Difference	Standard Deviation	Percent of Mean
A (m-K/W)	0.0452	0.06433	42.3%	0.00334	5.2%
B (m-K/W/K)	0.000246	0.0003230	31.3%	0.0000040	1.2%
E (W-K/m)	3.50E+09	1.950E+09	44.3%	0.207E+09	10.6%
F (K)	16361	12079.9	26.2%	192.5	1.6%
f(Bu)	0.00187	0.000945	49.5%	0.000010	1.0%
0.9 Factor	0.9	0.60	33.3%	0.15	24.9%
0.04 Factor	0.04	0.042	5.0%	0.013	30.5%
$g(Bu)_A$	0.038	0.0373	1.8%	0.0089	23.7%
$g(Bu)_B$	0.28	0.289	3.2%	0.053	18.5%
h(T)	396	350.2	11.6%	107.8	30.8%
Q	6380	4418.9	30.7%	253.5	5.7%

Table 12: Objective function evaluations associated with the mean parameter values from the MCMC analysis (irradiated fuel parameters / data only)

Analysis	$E_{\mathrm{RMS}}(\boldsymbol{\theta})$	Relative Improvement (%)
Nominal	7.19	-
MCMC (50%)	9.41	-30.9%

Figure 8 presents the posteriors associated with the MCMC analysis. Of concern are the rather dramatic changes of the posteriors associated with the first, third, and fourth parameters, as compared to those presented in Figure 7. The posterior associated with the first parameter changes from a Gaussian-like distribution to an Exponential-like distribution, and those associated with the third and fourth parameters change from "favoring" the upper to the lower bound. This is a particularly disturbing result, as it indicates that the two data sets associated with the fresh and irradiated fuel samples may not support the use of common values for the first four parameters of the FRAPCON model. In the very least, the independent calibrations of the model against data sets associated with fresh and irradiated fuel samples should be conducted with caution.

Of additional concern is the fact that the seventh through eleventh parameters exhibit posteriors that, for the most part, span the entire permissible ranges of the parameter values. Nonetheless,

there exist two strong correlations between the eighth ($g(Bu)_A$) and ninth ($g(Bu)_B$) parameters (negative) and between the tenth ($h(t)$) and eleventh (Q) parameters (positive). Again, these correlations are explained by Equation (8), but it is again unknown whether or not these will persist in MCMC Analysis (c); for example, the correlation between the first (A) and second (B) parameters is negligible in this analysis, where it was relatively strong in the previous analysis.

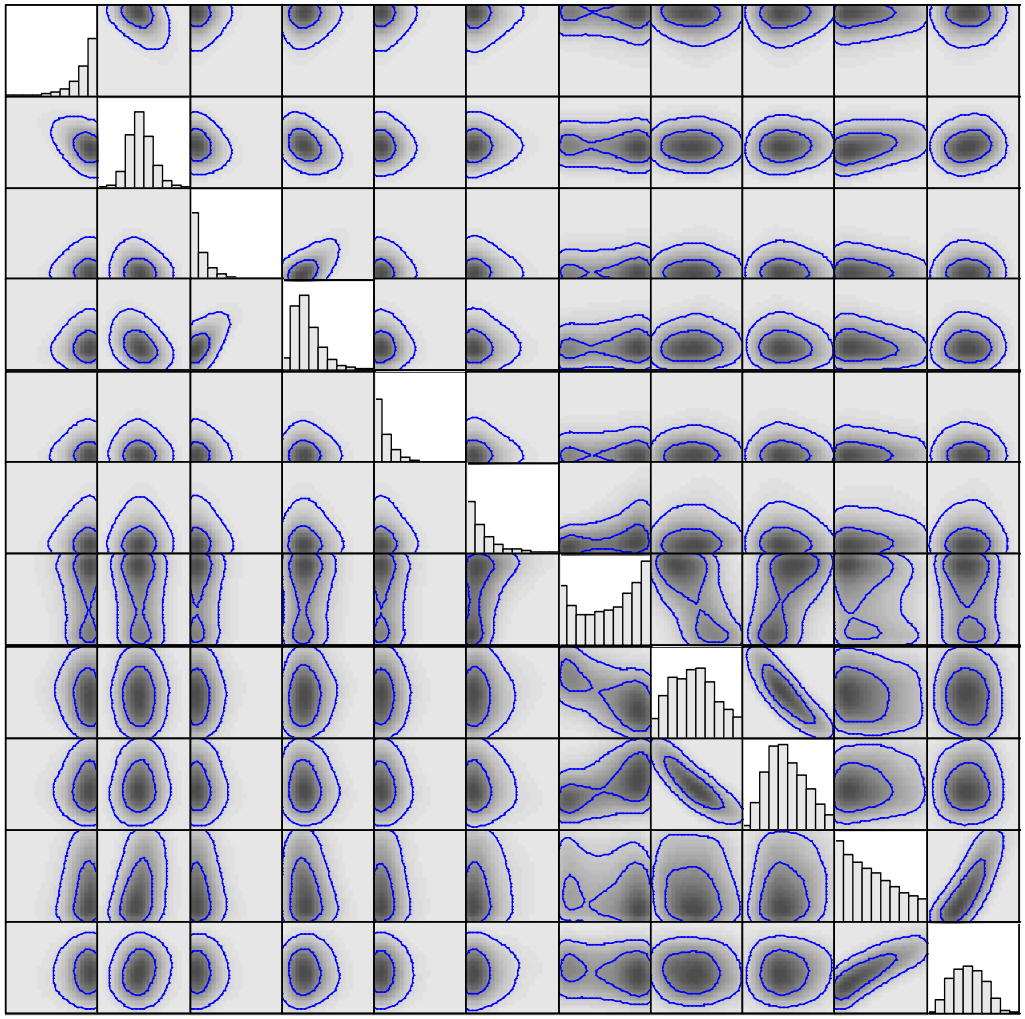

Figure 8: Estimates of univariate (diagonal) and bivariate (off-diagonal) marginal posterior distributions for MCMC Analysis (b)

As in Section 2.2.2, the authors employ the first four parameters presented in Table 11 to make predictions of the thermal conductivities associated with the fresh fuel samples. The result only goes to confirm the conclusion from Section 2.2.2 in that employing data associated with irradiated fuel samples alone for calibration of the FRAPCON model, does not yield a predictive model.

Table 13: Objective function evaluations associated with the mean parameter values from the MCMC analysis (fresh fuel parameters, irradiated data)

Analysis	$E_{\mathrm{RMS}}(\boldsymbol{\theta})$	**Relative Improvement (%)**
Nominal	5.22	-
MCMC (50%)	19.62	-275.8%

3.1.3 Data / Models for Fresh *and* Irradiated Fuel Samples

The attractiveness of this analysis is that it represents the only analysis reported upon that *simultaneously* considers all of the data / models. This is particularly interesting in that it allows for the comparison of the posteriors generated by this analysis with those of the previous two analyses, in which only the data / models for the fresh or irradiated fuel samples were considered separately. The first of these two comparisons is presented in Figure 9, where it is seen that the posteriors are nearly identical between MCMC Analyses (a) and (c). Likewise, the mean parameter values derived from both analyses are also nearly identical (see Table 9 and Table 16), which leads to nearly identical values reported for the $E_{\mathrm{RMS}}(\boldsymbol{\theta})$ associated with the fresh fuel samples (*i.e.* $E_{\mathrm{RMS}}(\boldsymbol{\theta}) = 4.46$ vs. $E_{\mathrm{RMS}}(\boldsymbol{\theta}) = 4.43$ in the MCMC Analysis (a)).

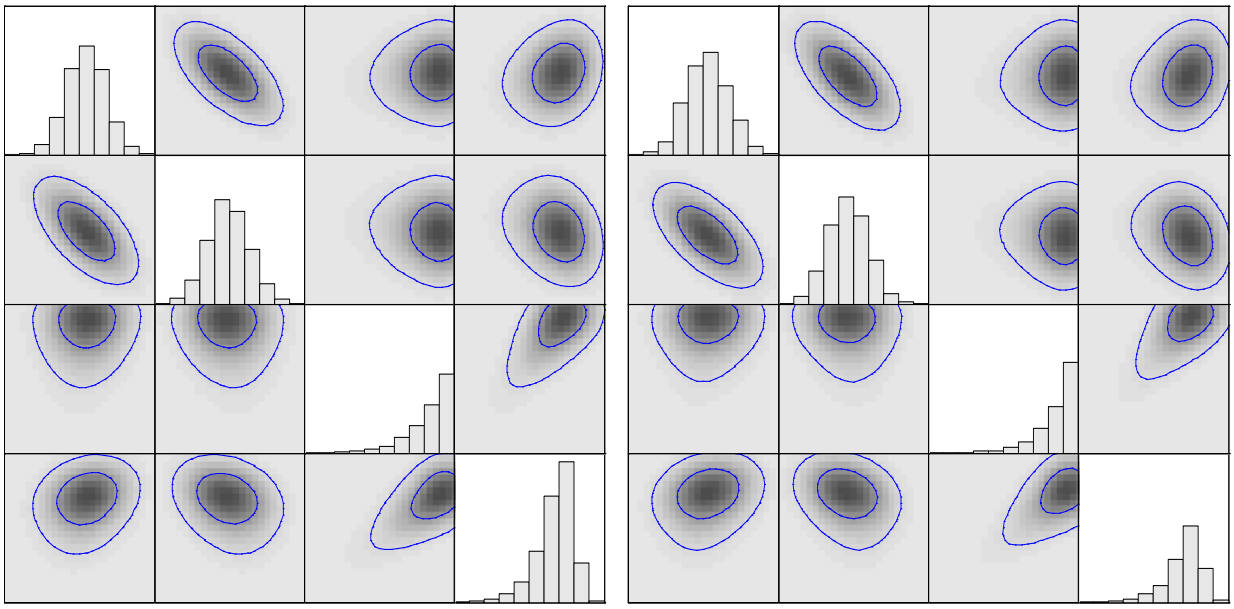

Figure 9: Comparison of univariate (diagonal) and bivariate (off-diagonal) marginal posterior distributions from MCMC Analyses (a) and (c)

Table 14: Objective function evaluations associated with the mean parameter values from the MCMC analysis (fresh fuel parameters, fresh *and* irradiated data)

Analysis	$\boldsymbol{E_{\mathrm{RMS}}(\theta)}$	**Relative Improvement (%)**
Nominal	5.22	-
MCMC (50%)	4.46	14.5%

Of more interest, however, is the comparison of the posteriors associated with *uncommon* parameters (*i.e.* the fifth through eleventh parameters). For this, the authors turn to comparing the posteriors resulting from MCMC Analyses (b) and (c), which are presented in Figure 10. Most obvious is the fact that variances on the posteriors associated with the sixth through eleventh parameters are significantly reduced. That is, the inclusion of data associated with fresh fuel samples in this combined analysis, has a dramatic effect on the values of parameters that *do not* pertain to fresh fuel samples. Recalling the comparison plots between experimental data and nominal model predictions for both fresh and irradiated fuel samples (see Figure 3 and Figure 5, respectively), this is not, in fact, an unexpected result. As noted previously, the nominal model associated with the fresh fuel samples offers a reasonably accurate representation of the available data (see Figure 3). Analogously, MCMC Analysis (a) generated posteriors that were significantly more informative than the assumed Uniform priors. Turning now to the nominal model associated with the irradiated fuel samples, it was noted that the fit of the model to the data was very poor (see Figure 5), which translated into the rather uninformative posteriors generated by MCMC Analysis (b).

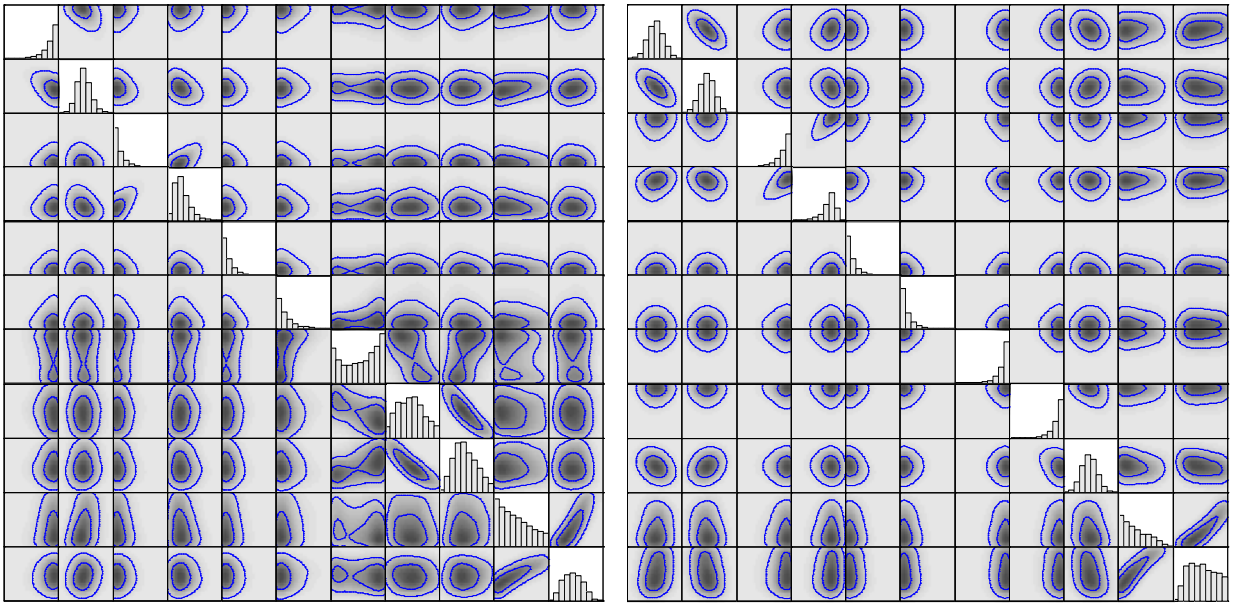

Figure 10: Comparison of univariate (diagonal) and bivariate (off-diagonal) marginal posterior distributions from MCMC Analyses (a) and (c)

Table 15: Objective function evaluations associated with the mean parameter values from the MCMC analysis (irradiated fuel parameters, fresh *and* irradiated data)

Analysis	$\boldsymbol{E_{\mathrm{RMS}}(\theta)}$	**Relative Improvement (%)**
Nominal	7.19	-
MCMC (50%)	7.80	-8.5%

Returning to MCMC Analysis (c), these previous two MCMC analyses essentially explain the changes seen in the posteriors associated with the sixth through eleventh parameters. The uninformed posteriors associated with MCMC Analysis (b) do not indicate strong tendencies for particular parameter values. So, when the relatively informed posteriors associated with MCMC Analysis (a) *do* indicate such tendencies, the remaining seven, uninformed parameters that are not common between the data / models must "fit" into this new scenario, in which the first four parameters are effectively fixed. That said, these tightened posteriors and in particular, their means (see Table 16), are far from the associated nominal parameter values, which only confirms the authors' conclusions from Sections 2.2.2 and 3.1.2.

Table 16: Mean parameter values from MCMC Analysis (c), allowing **50%** deviation from the nominal parameter values

Parameter Name	**Nominal Value**	**MCMC Mean Value**	**Percent Difference**	**Standard Deviation**	**Percent of Mean**
A (m-K/W)	0.0452	0.04997	10.6%	0.00159	3.2%
B (m-K/W/K)	0.000246	0.0002330	5.3%	0.0000017	0.7%
E (W-K/m)	3.50E+09	5.078E+09	45.1%	0.166E+09	3.3%
F (K)	16361	17540.6	7.2%	97.9	0.6%
f(Bu)	0.00187	0.000942	49.6%	0.000007	0.7%
0.9 Factor	0.9	0.46	48.9%	0.01	1.4%
0.04 Factor	0.04	0.060	50.0%	0.0004	0.7%
$g(Bu)_A$	0.038	0.0567	49.2%	0.0003	0.5%
$g(Bu)_B$	0.28	0.238	15.0%	0.003	1.1%
h(T)	396	315.9	20.2%	88.6	28.1%
Q	6380	8806.9	38.0%	396.2	4.5%

4 Info-Gap Decision Theory Analyses

The final assessment technique highlighted in this report adopts a framework anchored in *Info-Gap Decision Theory* (IGDT). Simply stated, IGDT offers a theoretical framework that aims to facilitate decision-making in the face of severe uncertainty [14]. A typical IGDT analysis aims to quantify the "info-gap robustness" of a series of decisions, ultimately providing the decision-maker with a series of so-called "robustness curves." These robustness curves illustrate, for each decision, the relationship (or trade-off) between the *performance* of a decision and the *robustness* against the uncertainty that contaminates the decision. Rounding out the analysis, the decision-maker defines a minimum performance requirement (*e.g.* maximum error) that then imposes a ranking of the decisions according to how robustly they meet that performance requirement.

For the purposes of this report, IGDT will be employed in a manner that is more analogous to a sensitivity analysis than a traditional info-gap analysis. However, as pointed out in [15], "the advantage of estimating sensitivities by way of an IGDT analysis is that we do not rely on approximating local or global derivatives or adjoints; IGDT produces sensitivities that are free of these limiting assumptions." To this end, the following discussion serves to provide a more detailed overview of IGDT, where the authors are quick to note that much of the following discussion has already been presented in [15]. This discussion is necessarily more thorough than the discussions provided in Sections 2 and 3, given the authors' perception that IGDT is a relatively new theory, particularly to the UQ community. Moreover, the authors will make every effort to maintain the general treatment of IGDT, as provided in [15], as such a treatment will facilitate the use of IGDT to solve a broader class of problems faced by UQ researchers. Interested readers are pointed toward [14] for a complete treatment of IGDT as well as the references contained in [16] for examples of how IGDT may be applied to various problems and problem types.

Any IGDT analysis begins with three central questions: (1) "What is the decision that needs to be made?" (2) "Where is the uncertainty that affects the quality of this decision?" (3) "How is the quality (or performance) of this decision quantified?" In this study, the decision we wish to inform through the IGDT analysis is whether or not the FRAPCON model remains predictive when its empirically-derived parameters are allowed to vary. Note that the previous sentence also answers the second question. The mechanism by which IDGT represents uncertainty is formally referred to as an "info-gap model of uncertainty." This representation is not necessarily a probabilistic model, as might be implied by the term "uncertainty." As info-gap implies, uncertainty is simply represented as a gap in information, about which little is assumed other than how it relates to the "nominal model" of the system. Oftentimes, these nominal models are derived by analyzing experimental data, eliciting expert opinion, compiling consistent theories, or they may simply be educated guesses offered by the analyst. For the results reported upon herein, this nominal model corresponds to the FRAPCON model, as provided in [17]. Regardless of how the nominal model is defined, however, it is important for the reader to keep in mind that

such a model represents the situation in which no uncertainty is expected in the model parameters (a precariously optimistic view of the world, in the authors' opinions).

The third and most subjective of the three questions is defined here to be consistent with the objective function defined for the optimization-based assessment in Section 2, repeated here for convenience:

$$E_{\mathrm{RMS}}(\boldsymbol{\theta}) = \sum_{i=1}^{n}\left(\frac{1}{m_n}\sum_{j=1}^{m_n}\left(K_{i,j}^{\exp} - K_{i,j}^{\mathrm{mod}}(\boldsymbol{\theta})\right)^2\right)^{1/2}. \tag{16}$$

Note that while a measure of accuracy is being employed in this study, this need not always be the case for IGDT analyses. Generally speaking, performance could be defined as a response feature that is not to exceed a certain threshold value (*e.g.* the deflection of a cantilevered beam) or as relating to efficiency of a decision (*e.g.* the time required to exercise a computer code or code segment).

Therefore, the IGDT analysis contained herein addresses the question: "What is the permissible level of ignorance about the parameters comprising the FRAPCON model that can be tolerated, which does not cause the predictions to exceed a maximum allowable level of error." This question is obviously of considerable importance when asked within the context of model calibration, since, as mentioned in Section 2, such calibrations are often done without regard to what the parameter variations mean, leading to models that fit the experimental data but may exhibit little-to-no predictive capability. This discussion proceeds in Section 4.1 with a more formal treatment of the IGDT problem formulation.

4.1 Problem Formulation

The IGDT problem formulation begins generally, by considering a set of analytical models $\boldsymbol{\mathcal{M}}$, all of which describe the thermal conductivity of fresh and/or irradiated UO_2 fuel pellets. From $\boldsymbol{\mathcal{M}}$ are chosen M models $m_I(\boldsymbol{\theta}^{m_I})\forall I = 1,2,\ldots,M$, where $\boldsymbol{\theta}^{m_I}$ is a column vector that collects the parameters for the $m_I{}^{\text{th}}$ model, and $\tilde{\boldsymbol{\theta}}^{m_I}$ denotes the nominal model parameters associated with the $m_I{}^{\text{th}}$ model. Note that the length of the vectors $\boldsymbol{\theta}^{m_I}$ need not be consistent across the M analytical models.

Having provided the above definitions, the info-gap model of uncertainty may be defined as

$$\boldsymbol{\mathcal{U}}(m_I,\alpha) = \left\{\boldsymbol{\theta}^{m_I}: \left|\frac{\boldsymbol{\theta}_j^{m_I} - \tilde{\boldsymbol{\theta}}_j^{m_I}}{\tilde{\boldsymbol{\theta}}_j^{m_I}}\right| \le \alpha, \forall j\right\}, \alpha \ge 0. \tag{17}$$

Equation (17) is representative of a class of info-gap models referred to as "envelope-bound" (or "error-bound") info-gap models [14], and $\boldsymbol{\mathcal{U}}(m_I,\alpha)$ represents a *nested set* of m_I-type analytical models, whose parameters may assume values within the bounded interval defined by α: an

unknown scalar quantity, referred to as the "horizon-of-uncertainty." This simply means that the extent to which the model parameters can deviate from their nominal values is, in actuality, unknown (though practically speaking, decision analysts will often set limits). Put another way, Equation (17) explicitly defines *sets* of model parameters from which the analyst may choose, given a fixed level of the horizon-of-uncertainty (or level of lack of knowledge). As the level of lack of knowledge increases, the set of potential parameter values also grows.

As a further aid to the reader, a representative illustration of an envelope-bound info-gap model is presented in Figure 11 where it is seen that at $\alpha = \alpha_2$, the range of values that the parameter labeled b_i^{u} may assume also includes that defined at $\alpha = \alpha_1$. Likewise, the range of values that b_i^{u} may assume at $\alpha = \alpha_3$, includes that defined at $\alpha = \alpha_2$. This illustration does not imply that an info-gap model of uncertainty is limited to nested intervals. The parameter b_i^{u} could, for example, represent the standard deviation or entropy of a family of probability laws that describe variability.

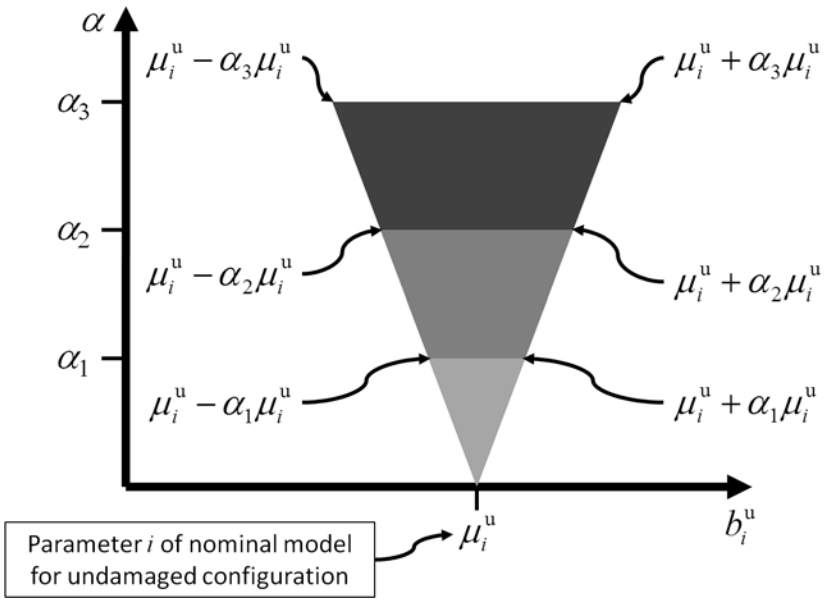

Figure 11: Representative illustration of the nested nature of Equation (17)

With the info-gap model of uncertainty (*i.e.* Equation (17)) and the performance function (*i.e.* Equation (16)) defined, the central concepts of IGDT, namely "robustness" and "opportunity," may be introduced. Simply stated, robustness is a reflection of the immunity of the model(s) to uncertainty in the model form or its parameters [14]. In the present context, highly robust models will have two characteristics: (a) acceptable agreement between the nominal response features predicted by $m_I\left(\widetilde{\boldsymbol{\theta}}^{m_I}\right)$ and the experimental data and (b) little change in the evaluation of Equation (16) over the set defined by Equation (17). Conversely, analytical models with low levels of robustness violate one or both of the above characteristics. Clearly, higher robustness is

better than lower robustness at a similar level of performance; this observation offers the mechanism for model selection.

Opportunity then relates to the potential to *improve* the performance of a model, given uncertainty in the functional form or parameters that define that model. Considering the problem of model calibration, the nominal model may be thought of as an initial, best guess at the values of the parameters. Subsequently, the calibration will lead to "improved" definitions of these parameters such that the model predictions better fit the available experimental data. Opportunity would uncover this potential, but it should not be considered as analogous to calibration; the intent of IGDT is only to inform the decision-making process.

The robustness and opportunity functions are formally stated as

$$\hat{\alpha}(m_I, E_c) = \max_{\alpha}\left\{\max_{\boldsymbol{\theta}^{m_I}\in \boldsymbol{U}(m_I,\alpha)}\{E_{\mathrm{RMS}}(\boldsymbol{\theta})\} \le E_c\right\} \tag{18}$$

and

$$\hat{\beta}(m_I, E_c) = \max_{\alpha}\left\{\min_{\boldsymbol{\theta}^{m_I}\in \boldsymbol{U}(m_I,\alpha)}\{E_{\mathrm{RMS}}(\boldsymbol{\theta})\} \ge E_c\right\}, \tag{19}$$

respectively. Equation (18) that defines the robustness function has two parts: an inner maximum and an outer maximum. The inner maximum reflects the worst-case performance of the family of models defined by $m_I(\boldsymbol{\theta}^{m_I})$, where the parameters $\boldsymbol{\theta}^{m_I}$ are selected from the set $\boldsymbol{U}(m_I, \alpha)$. Even though the robustness function identifies the worst-case performance within the family of models, the inequality of Equation (18) guarantees that this worst fidelity to data does not exceed the level E_c of prediction error. Therefore, E_c, which is a threshold selected by the analyst, can be understood as being a requirement for prediction accuracy. Incorporating this inner maximum, the outer maximum is then interpreted as seeking the maximum value of the horizon-of-uncertainty α, for which the worst-case performance of the analytical model does not exceed a critical level E_c.

While this knowledge is useful, in a practical application, it can be of far more benefit to the decision analyst to plot the inner maximum for various values of the horizon-of-uncertainty α, producing the aforementioned "robustness curve." Such curves then provide the decision analyst with insight as to how the worst-case performance of a family of models varies with increasing levels of lack of knowledge. In cases where multiple models are considered, the respective robustness curves may be overlaid allowing the decision analyst to weigh the merits of each model relative to others. An example of such a set of robustness curves is presented in Figure 12. The black, dashed line of Figure 12 follows the most robust model, starting with the model labeled m_3, then switching over to the model labeled m_2, as the horizon-of-uncertainty α increases.

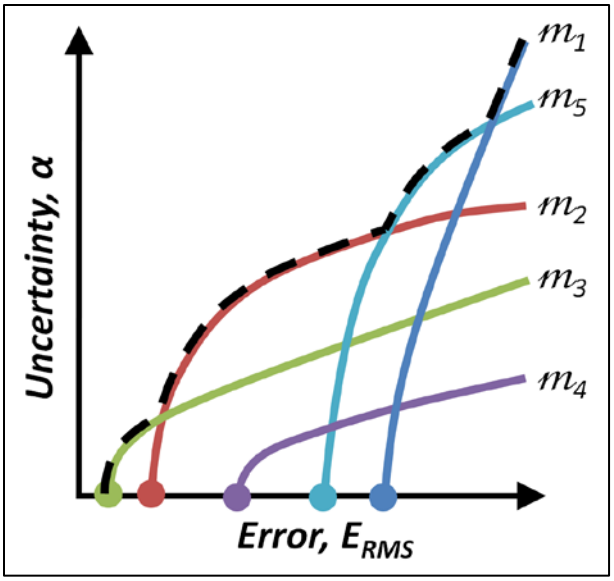

Figure 12: Robustness curves for a set of five hypothetical models

Despite being a hypothetical example, Figure 12 demonstrates several results that may arise from IGDT analyses. First is the idea that each of the five models demonstrates zero robustness when they assume the nominal model parameters. This is analogous to an analyst employing his/her best guess at the model parameters, executing each model once, and treating the model exhibiting the least error as *the* answer to the problem. It is the authors' contention that such a stance represents a precariously optimistic view of the world, as epistemic uncertainty (*i.e.* a lack of *complete* knowledge about the behavior of the system) is present, but ignored when the model is analyzed only once. A reflection of this lack of knowledge is demonstrated in the non-zero errors produced by nominal models. That is, nominal models are incorrect, not necessarily because the analyst employed incorrect assumptions about the parameters, but possibly because the *form* of the model does not capture the full spectrum of system behavior.

The second result illustrated by Figure 12 is that of model preference reversal. That is, as the level of uncertainty increases, the worst-case performances predicted by the different models do not change at the same rates, resulting in crossing of the robustness curves. It is noted that crossing does not always occur; robustness curves can follow parallel or divergent tracks such that crossing cannot occur. Examination of Figure 12 reveals three levels of lack of knowledge where crossing of the robustness curves occurs. Faced with this situation, the decision analyst may choose the model that satisfies the minimum performance requirement, but admits the most lack of knowledge, as compared to the other models. This choice guarantees that predictions of the model meet the minimum performance requirement, even if some of the model parameters are selected erroneously. Alternatively, the decision analyst may assume a level of uncertainty and subsequently choose the model that offers the least error at that uncertainty. It may, however, be argued that the latter interpretation of the robustness curve is less aligned with the spirit of IGDT. An important message associated with the idea of model preference reversal is that the

model that produces the least prediction error may not be the best choice, if one is also uncertain about the functional form or parameters that comprise the model. That is, the so-called optimal model may become sub-optimal in the face of uncertainty, when compared against an alternative modeling strategy. This goes to the authors' earlier assertion that optimization-based calibration often does not provide a complete picture of the problem.

Equation (19) presents the converse of the robustness function: the opportunity function. It is noted that the only difference between the Equations (18) and (19) is that the inner maximum in Equation (18) becomes an inner minimum in Equation (19). Translated into English, this inner minimum seeks the best-case performance of the analytical model defined by $\mathcal{m}_I(\boldsymbol{\theta}^{m_I})$, where the parameters $\boldsymbol{\theta}^{m_I}$ are selected from the set $\boldsymbol{\mathcal{U}}(\mathcal{m}_I, \alpha)$. This presents the situation where uncertainty about the parameters comprising a model can *improve* the performance of that model, as compared to the nominal condition, a situation referred to as "windfalling" [14]. Such knowledge could be used to inform calibration studies by quantifying the extent to which prediction accuracy could potentially be improved.

Ultimately, the question of whether to assess robustness or opportunity comes down to a question of whether the analyst is pessimistic or optimistic about his/her model. It is the authors' opinion that more often than not, analysts will wish to examine robustness. Consider, for example, a model that approximates a physical system known to have considerable implications with respect to life-safety. In this situation, analyzing opportunity would be of little-to-no use, given that few decision-makers (*e.g.* regulatory agencies, policy-makers) would formulate policies from knowledge of best-case scenarios. With that said, having knowledge of the opportunity of a decision (*e.g.* a model) at various levels of lack of knowledge can present the analyst with valuable insight.

4.1.1 Robustness of Individual Model Parameters

The previous discussion provides a reasonably complete introduction to info-gap decision theory, but as mentioned, the results discussed in Section 4.2 emanate from a less-than-traditional application of IGDT. This does not, however, imply that the previous discussion is superfluous. On the contrary, the IGDT framework as outlined above is applicable to any problem where uncertainty clouds a decision aimed at selecting a model: an all too common in the scientific and engineering community. Moreover, in the absence of the context provided by the previous discussion, the following would have little meaning.

The "less-than-traditional application of IGDT" primarily refers to an extension of the framework outlined previously to also compute robustness and opportunity functions that are specific to a single parameter. To accomplish this, the info-gap model in Equation (17) is modified such that all of the uncertain model parameters are held fixed at their nominal values, except for the k^{th} parameter. Equation (20) presents this modified info-gap model of uncertainty as

$$\boldsymbol{\mathcal{U}}_k(m_I,\alpha)=\left\{\boldsymbol{\theta}^{m_I}:\left\{\begin{array}{c}\boldsymbol{\theta}_j^{m_I}=\widetilde{\boldsymbol{\theta}}_j^{m_I},\forall j\neq k\\ \left|\dfrac{\boldsymbol{\theta}_k^{m_I}-\widetilde{\boldsymbol{\theta}}_k^{m_I}}{\widetilde{\boldsymbol{\theta}}_k^{m_I}}\right|\leq\alpha\end{array}\right\}\right\},\alpha\geq 0. \tag{20}$$

While this imposes additional computational expense to the info-gap analysis (especially for models having many parameters), evaluating Equations (18) and (19) subject to the constraint imposed by Equation (20) allows the analyst to examine the influence of *individual* uncertain parameters on the robustness or opportunity function. The results of such an exercise can be viewed as analogous to a main-effect sensitivity analysis, where the sensitivity is assessed with respect to the performance function of Equation (16). It is worth repeating that the advantage of estimating sensitivities by way of an IGDT analysis is that there is no reliance on approximating local or global derivatives (or adjoints). Moreover, the IGDT treatment of uncertainty is both general and flexible in that most any type of uncertainty (probabilistic or otherwise) can be handled by way of an IGDT analysis.

4.2 Results

As for Section 2.2, the results presented in this section are organized around two sub-sections that pertain to two combinations of data sets and model parameters. Section 4.2.1 pertains to thermal conductivity data associated with fresh fuel samples, which is analyzed using the FRAPCON-3.4 thermal conductivity model given by Equation (2). Section 4.2.2 then pertains to thermal conductivity data associated with irradiated fuel samples, which is analyzed using the FRAPCON-3.4 thermal conductivity model given by Equation (8).

4.2.1 Data / Model for Fresh Fuel Samples

This discussion begins by considering the effect on performance (*i.e.* fidelity to data) when all of the four empirically-derived parameters contained in Equation (2) are permitted to vary. Figure 13 illustrates the robustness curves that result from IGDT analyses using the info-gap models of uncertainty given by Equations (17) and (20). Note that for all of the figures in this section, the parameters are ordered as in Section 2.2; the table below is provided for clarity.

Table 17: Parameter labeling scheme for Section 4.2.1

Parameter Number	Parameter Name
1	A (m-K/W)
2	B (m-K/W/K)
3	E (W-K/m)
4	F (K)

The primary finding from this analysis is that above approximately $\alpha \cong 15\%$ the overall "worst case performance"[5] of the FRAPCON model (solid, blue line) degrades severely, going from $E_{\mathrm{RMS}}(\boldsymbol{\theta}) \cong 14$ at $\alpha \cong 15\%$ to $E_{\mathrm{RMS}}(\boldsymbol{\theta}) \cong 28$ at $\alpha \cong 25\%$. This degradation in performance appears to be, in large part, tied to the variation of the fourth parameter, which is made more obvious by the "influence curves" presented in Figure 14.

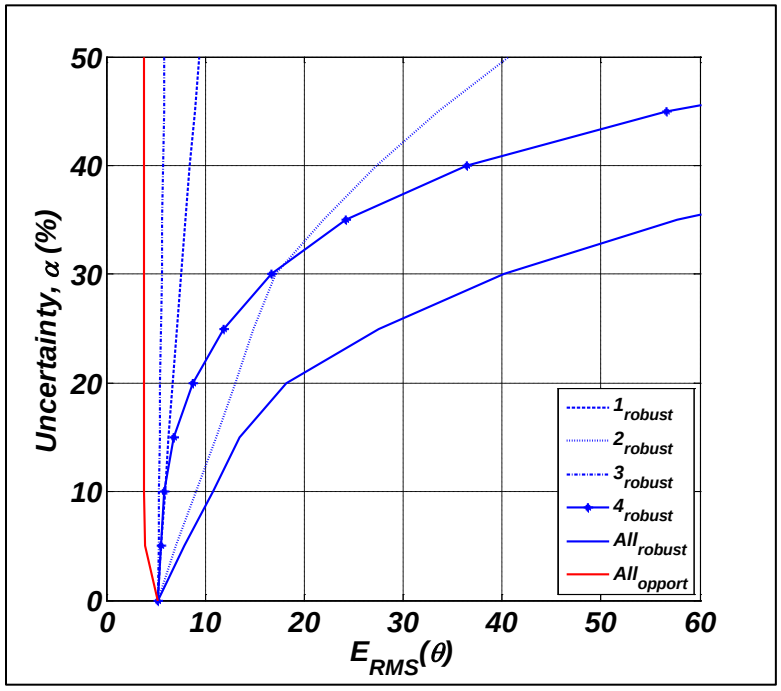

Figure 13: Robustness curves from the **four**-parameter case

[5] The authors note that the phrase "worst case performance" is conditioned on a particular value of α. Technically-speaking, a worst case performance does not exist in the context of IGDT, as α is defined simply as an *unbounded* scalar that modulates the space(s) defined by the info-gap models of uncertainty. Practically-speaking, of course, evaluating Equations (15) and (16) requires the definition of α, so the authors use "worst case performance" with this fact in mind.

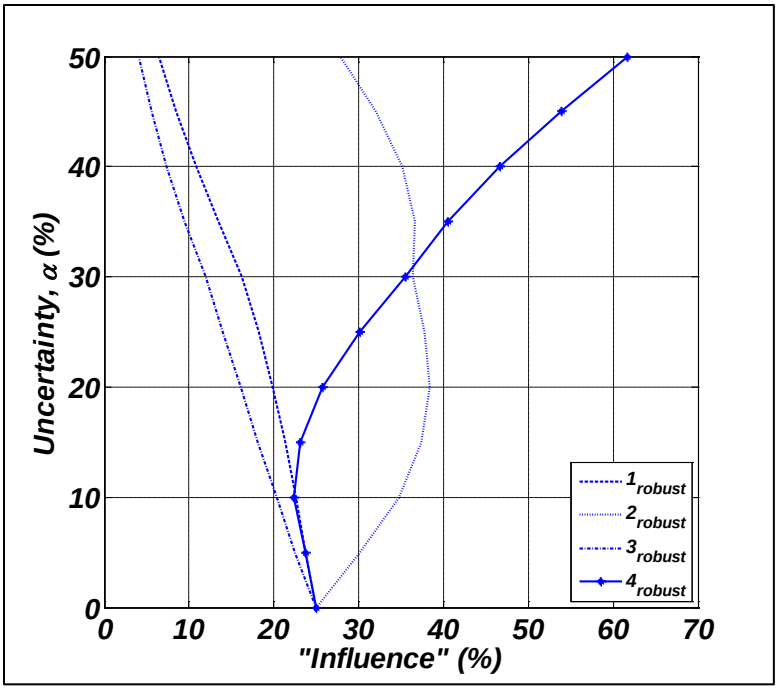

Figure 14: Influence curves from the **four**-parameter case

Effectively, influence is computed by normalizing the robustness curves that result from the IGDT analyses associated with Equation (20). To begin, the inner maximum from Equation (18) is denoted as $\gamma(m_I, \alpha)$, where it is pointed out that this quantity (for various values of α) is, in fact, the quantity plotted in Figure 13 as the solid, blue line ("$\text{All}_{\text{robust}}$"). The analogous inner maximum associated with IGDT analysis of the k^{th} parameter is then denoted as $\gamma_k(m_I, \alpha)$. Finally, a formal statement of influence is given as

$$I(m_I, \alpha) = \frac{\gamma_k(m_I, \alpha)}{\sum_{k=1}^{N} \gamma_k(m_I, \alpha)}. \tag{21}$$

where N is the number of parameters considered in the IGDT analyses associated with Equation (20). Examining Figure 14, it is seen that at approximately $\alpha \cong 15\%$, the fourth parameter becomes more influential (and the second parameter becomes *less* influential), eventually accounting for approximately 62% of the summation $\sum_{k=1}^{N} \gamma_k(m_I, \alpha)$ at $\alpha = 50\%$. Recalling the results from Section 2.2.1 in which GA-optimized value of the fourth parameter deviated only slightly from its nominal value (even when the allowable deviation was set at 50%), the results illustrated by Figure 14 appear to be consistent, in that significant variation of the fourth parameter may lead to poor performance. The converse of this hypothesis also seems likely, as the parameter that varied the farthest from its nominal value in the GA optimization (*i.e.* the third parameter) also exhibits the least influence in Figure 14.

In light of this knowledge, the authors chose to execute a similar analysis as the above, except that the fourth parameter was not included in the analysis. Arguably, the most important conclusion from this re-analysis derives from Figure 15, in that the performance degradation of the FRAPCON model is less dramatic as compared to the four-parameter case. This is not an unexpected result, however, as removing one or more parameters that are correlated with one or more of the remaining parameters will likely result in an improvement of performance (due to the reduced space over which the optimization is performed).

This analysis also represents an example of how the decision-maker could use the results of a previous IGDT analysis to inform a follow-on analysis. In the present case, the authors asserted that a majority of the performance degradation of the FRAPCON model was due to variation of the fourth parameter, where the obvious action of such a finding would be to reduce or eliminate the allowable variation of the fourth parameter. Having taken such an action, however, the decision-maker may yet be interested in how this alters the overall robustness of the model (*i.e.* "How does the solid, blue line from Figure 13 change?"). It is expected that the overall robustness of the model would improve, but the degree to which this the robustness improves is left to question in the absence of a second IGDT analysis.

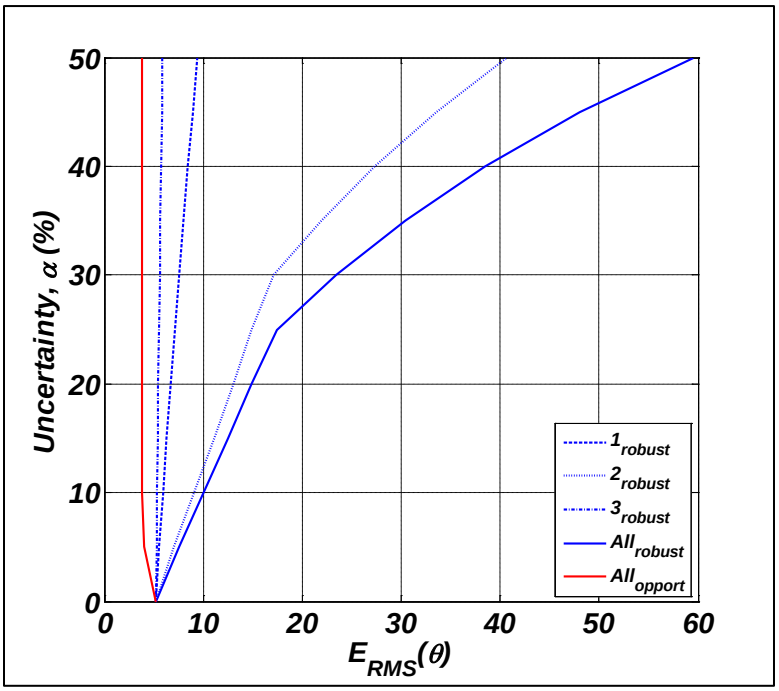

Figure 15: Robustness curves from the **three**-parameter case

4.2.2 Data / Model for Irradiated Fuel Samples

Analogously to the previous section, this discussion begins by considering the effect on performance (*i.e.* fidelity to data) when all of the *eleven* empirically-derived parameters

contained in Equation (8) are permitted to vary. Figure 16 illustrates the robustness curves that result from IGDT analyses using the info-gap models of uncertainty given by Equations (17) and (20). Note that for all of the figures in this section, the parameters are ordered as in Section 2.2; the table below is provided for clarity.

Table 18: Parameter labeling scheme for Section 4.2.2

Parameter Number	**Parameter Name**
1	A (m-K/W)
2	B (m-K/W/K)
3	E (W-K/m)
4	F (K)
5	f(Bu)
6	0.9 Factor
7	0.04 Factor
8	g(Bu) A
9	g(Bu) B
10	h(T)
11	Q

Upon examination Figure 16, a similar trend to that observed in the previous section is also observed here, in that the performance of the FRAPCON model degrades severely as uncertainty is introduced into the IGDT analysis. At first glance, this degradation again appears to follow as a result of varying the fourth parameter, but there are distinguishing characteristics that set this analysis apart from that of the previous section.

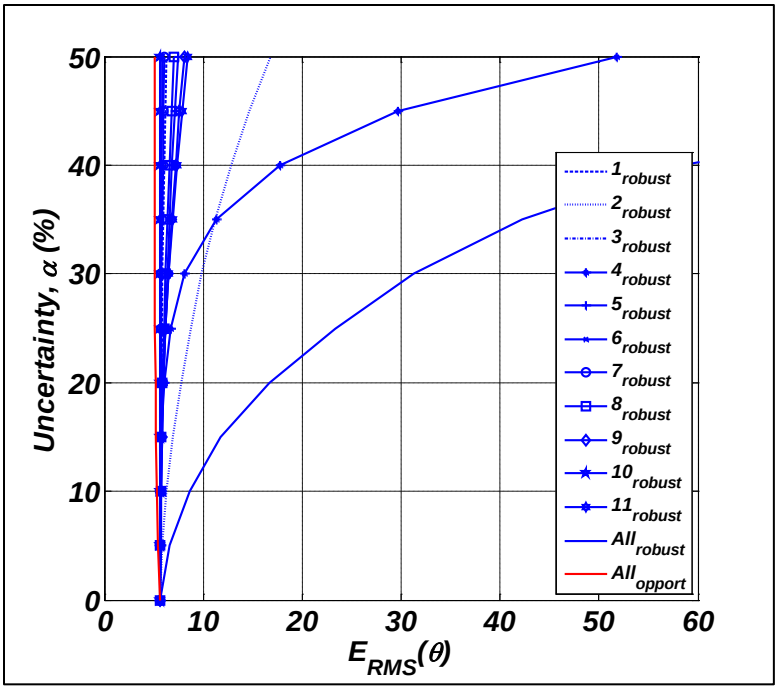

Figure 16: Robustness curves from the **eleven**-parameter case

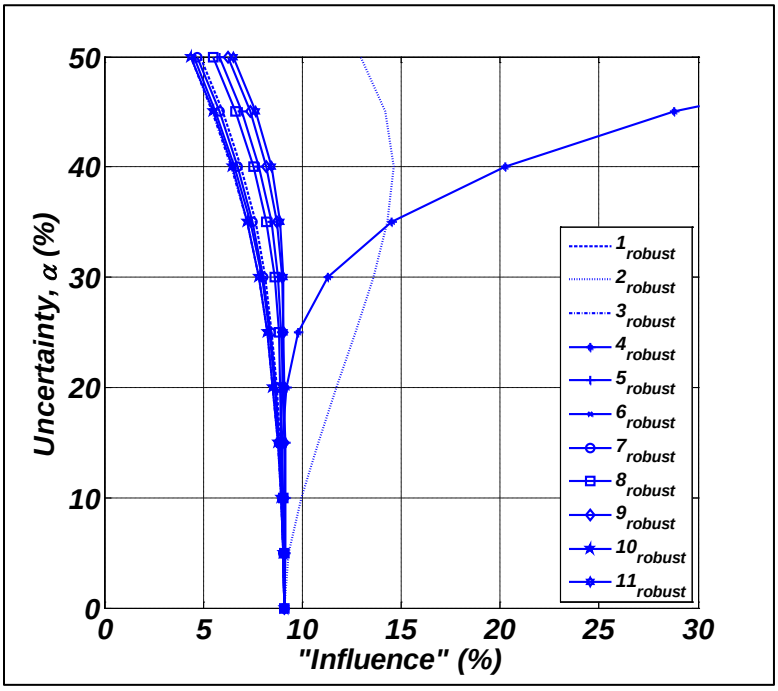

Figure 17: Influence curves from the **eleven**-parameter case

First, the uncertainty at which the fourth parameter becomes more influential (and the second parameter becomes *less* influential), relative to the other parameters (see Figure 17), is higher than in the previous section: $\alpha \cong 35\%$ in this section vs. $\alpha \cong 15\%$ in Section 4.2.1. This is most

probably a result of the fact that the model considered in this section contains an additional seven parameters. Related to this, the performance degradations associated with the second and fourth parameters at $\alpha = 50\%$ are not nearly as severe as in the previous section: for the second parameter, $E_{\mathrm{RMS}}(\boldsymbol{\theta}) \cong 17$ vs. $E_{\mathrm{RMS}}(\boldsymbol{\theta}) \cong 41$ and for the fourth parameter, $E_{\mathrm{RMS}}(\boldsymbol{\theta}) \cong 52$ vs. $E_{\mathrm{RMS}}(\boldsymbol{\theta}) \cong 90$. It is again noted that the performances referred to are "worst case performances," conditioned on a horizon of uncertainty of $\alpha = 50\%$.

Nevertheless, when $\alpha > 35\%$, the influence of the fourth parameter appears to be significant, and for that reason, the authors again executed an IGDT that did not include the fourth parameter, the results of which are presented in Figure 18. The primary finding of this analysis is simply that even in the absence of varying the fourth parameter, the degradation in performance of the FRAPCON model is still severe. Possibly with the exception of the second parameter, such degradation cannot be attributed to a particular parameter. In fact, the robustness curves in Figure 18 exhibit very high robustness (*i.e.* near negligible sensitivity to parametric uncertainty), yielding performances at $\alpha = 50\%$ that are only a few percent worse than the nominal performance of the model.

This finding is something of a double-edged sword, in that it illustrates that the FRAPCON model is robust to variation in *individual* parameters, but very sensitive to the simultaneous variation of *multiple* parameters. It seems that a reasonable follow-on study would be to consider combinations of parameters to determine whether varying a particular combination of parameters contributes to the majority of the performance degradation reported upon herein.

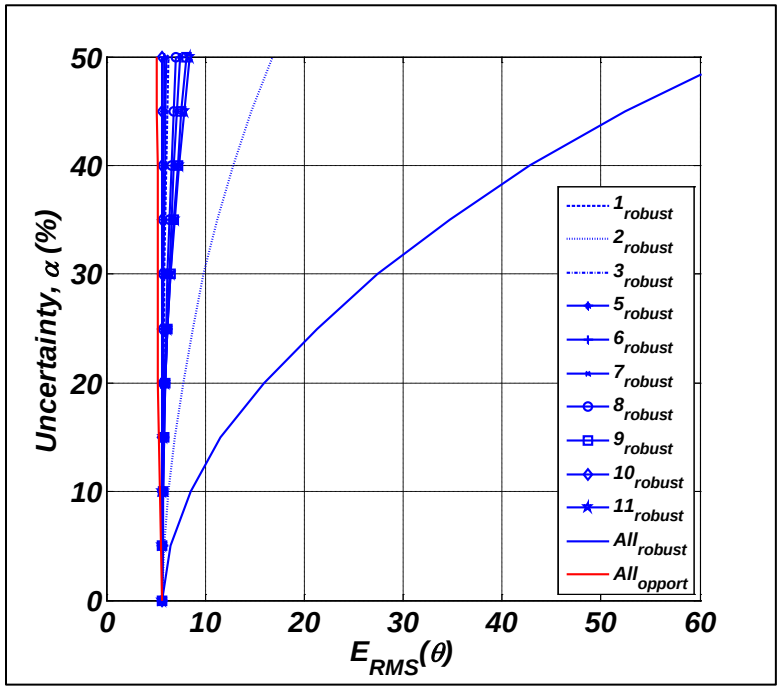

Figure 18: Robustness curves from the **ten**-parameter case

5 Preliminary Assessment of BISON Nuclear Fuel Performance Code

BISON [5] is a finite element-based, nuclear fuel performance code, applicable to a variety of fuel forms including light water reactor fuel rods, TRISO particle fuels, and metallic rod and plate fuels. It solves the fully-coupled equations of thermomechanics and species diffusion, for either two-dimensional axisymmetric or three-dimensional geometries. Fuel models are included to describe temperature- and burnup-dependent thermal properties, fission product swelling, densification, thermal and irradiation creep, fracture, and fission gas production and release. Plasticity, irradiation growth, and thermal and irradiation creep models are implemented for clad materials as well. Models are also available to simulate gap heat transfer, mechanical contact, and the evolution of the gap / plenum pressure with plenum volume, gas temperature, and fission gas addition. BISON is based on the MOOSE framework [6] and can therefore efficiently solve problems using standard workstations or very large high-performance computers.

The fuel performance modeled within BISON is driven by complex mechanisms that are only complicated by the effects of irradiation. It is very difficult to study a single model or even a subset of models, because all of the models interact with each other. The authors considered studying the fission gas release and thermal conductivity models initially, but due to the interdependencies, it was decided that the following six models within BISON would be studied. These are:

- Fission product swelling;
- Fuel relocation;
- Thermal and irradiation creep;
- Gap heat transfer;
- Thermal conductivity;
- Fission gas release.

Multiple parameters from each of six models are selected, for a total of 64 parameters. The numbers of parameters from each model are presented in Table 19. Unfortunately, the number of code execution failures[6] produced by varying the parameters associated with the fission product swelling and thermal and irradiation creep models further reduced the study to include only four models (*i.e.* fuel relocation, gap heat transfer[7], thermal conductivity, and fission gas release).

[6] A failure is denoted as a crash of the code due to an MPI error or an execution time that exceeds 20 minutes, where the nominal model required only 3 minutes to successfully execute.

[7] It is further noted that two of the four parameters associated with the gap heat transfer model could also not be varied, due to an inordinate number of failures, so only two parameters are considered for the gap heat transfer model.

Table 19: Selected models and number of parameters

Model	Number of Parameters
Fission product swelling	5
Fuel relocation	5
Thermal and irradiation creep	11
Gap heat transfer	4
Thermal conductivity	13
Fission gas release	26

For the purposes of this report, the authors will not discuss the details of these models, but will instead focus on the parameter screening studies performed as part of this preliminary assessment. For the details of these (and other) models implemented in BISON, the readers are directed to [5] and the references contained therein. It is noted however, that while the latest thermal conductivity model in FRAPCON-3.4 was examined in the previous sections of this report, this is *not* the model currently available in BISON. Instead, BISON employs the thermal conductivity models from [2] and [3], which are given as

$$K_{95,\text{fresh}} = \frac{100}{7.5408 + 17.692T + 3.6142T^2} + \frac{6400}{T^{5/2}} \exp\left(-\frac{16.35}{T}\right), \tag{22}$$

for the fresh fuel and

$$K_{95,\text{irrad}} = K_{95,\text{fresh}} \kappa_{1d} \kappa_{1p} \kappa_{2p} \kappa_{4r}, \tag{23}$$

for the irradiated fuel. In Equation (23), the multipliers κ_{1d}, κ_{1p}, κ_{2p}, and κ_{4r} account for dissolved fission products, precipitated solid fission products, pore and fission-gas bubbles, and radiation damage, respectively. For the details of these expressions, the readers are directed to [3] and the references contained therein. Table 20 through Table 23 provide the parameters (with nominal values), for each of the four models considered by the screening study discussed below.

Table 20: Parameters (with nominal values) varied in the BISON gap heat transfer model

Parameter Number	Parameter Name	Nominal Value
1	ROUGH_COEFF	2.57
2	CONTACT_COEFF	10.0

Table 21: Parameters (with nominal values) varied in the BISON fuel relocation model

Parameter Number	Parameter Name	Nominal Value
1	FUEL_RELOC_1	0.8
2	FUEL_RELOC_2	0.005
3	FUEL_RELOC_3	0.3
4	FUEL_RELOC_4	0.2
5	FUEL_RELOC_5	0.3

Table 22: Parameters (with nominal values) varied in the BISON thermal conductivity model ("FINK_" prefix denotes fresh fuel samples, "LUCUTA_" denotes multipliers for irradiated fuel samples)

Parameter Number	Parameter Name	Nominal Value
1	FINK_EQN19_1	1.00E-05
2	FINK_EQN19_2	1.0E-07
3	FINK_EQN19_3	1.0E-08
4	FINK_EQN19_4	5E-07
5	FINK_EQN19_5	0.287
6	FINK_EQN19_6	0.626
7	LUCUTA_EQN7a	0.5
8	LUCUTA_EQN7b_1	1.00E+07
9	LUCUTA_EQN7b_2	0.001
10	LUCUTA_EQN10b_1	0.3017
11	LUCUTA_EQN10b_2	1.0
12	LUCUTA_EQN11b	24
13	LUCUTA_EQN14f	0.2

Table 23: Parameters (with nominal values) varied in the BISON fission gas release model ("GR_" prefix denotes gas release, "DC_" prefix denotes diffusion coefficient)

Parameter Number	Parameter Name	Nominal Value
1	GR_GRAIN_RAD	1.00E-05
2	GR_RESOL_RATE	1.0E-07
3	GR_RESOL_DEPTH	1.0E-08
4	GR_BUBBLE_RAD	5E-07
5	GR_BUBBLE_SHAPE_FACT	0.287
6	GR_SURF_TENSION	0.626
7	GR_FRAC_COVERAGE	0.5
8	GR_EXT_PRESSURE	1.00E+07
9	GR_RELEASE_FRAC	0.001
10	GR_FRAC_YIELD	0.3017
11	GR_CALIB_FACTOR	1.0
12	DC_BUBBLE_PER_FRAG	24
13	DC_FRAG_RANGE	6.0E-06
14	DC_FRAG_INFLUENCE	1.0E-09
15	DC_GAS_ATOM_DIFF_COEFF_1	7.60E-10
16	DC_GAS_ATOM_DIFF_COEFF_2	-35000
17	DC_GAS_ATOM_DIFF_COEFF_3	1.41E-25
18	DC_GAS_ATOM_DIFF_COEFF_4	-13800
19	DC_GAS_ATOM_DIFF_COEFF_5	2.00E-40
20	DC_INTRA_BUBBLE_RAD_1	5.0E-10
21	DC_INTRA_BUBBLE_RAD_2	106.0
22	DC_INTRA_BUBBLE_RAD_3	-8703
23	DC_INTRA_CAPTURE_RATE	4.0
24	DC_INTRA_RESOL_RATE	3.03
25	DC_B_DRREF	4E-14
26	DC_FRREF	9.21E+18

The remainder of this section focuses on a main effects and linear interaction effects screening conducted on the parameters listed in Table 20 through Table 23. The aim of this screening is to remove parameters that have little-to-no effect on the variance of the feature(s) of interest. For this analysis, the features of interest are the lower and upper thermocouple temperatures predicted by BISON at the end of the analysis (*i.e.* through "beginning of life" of the Halden IFA-432 Rod 1 fuel rod [18]).

The reduction in the number of parameters realized by the screening study is intended to permit a more thorough sensitivity analysis, where the remaining parameters are varied in order to determine statistical significance for future studies. Unfortunately, the sensitivity analysis that was conducted for this report was found to be inconclusive. It is the authors' opinion that more

fundamental issues, which are beyond the scope of this report, need to be addressed before a full calibration / validation study can be conducted on BISON. This is not necessarily a surprising result given that BISON is still a development code (that is very much actively being developed both by researchers at INL and by others).

Designs of (computer) experiments are constructed for each of the four models, allowing *ten percent* deviation from the nominal parameter values. The relatively small number of parameters associated with the gap heat transfer and fuel relocation models (*i.e.* 2 and 5, respectively) permitted the use of two-level, *full* factorial designs to study the statistical significance of the associated parameters. However, the relatively large number of parameters associated with the thermal conductivity and fission gas release models necessitated an alternate strategy. To this end, the authors constructed two-level, *fractional* factorial designs, that were constrained by the number of BISON executions (in this case, 64). These latter designs were generated using the MATLAB™ functions `fracfactgen()` and `fracfact()`. Figure 19 through Figure 21 present overviews of the main effects analyses associated with each of the four models.

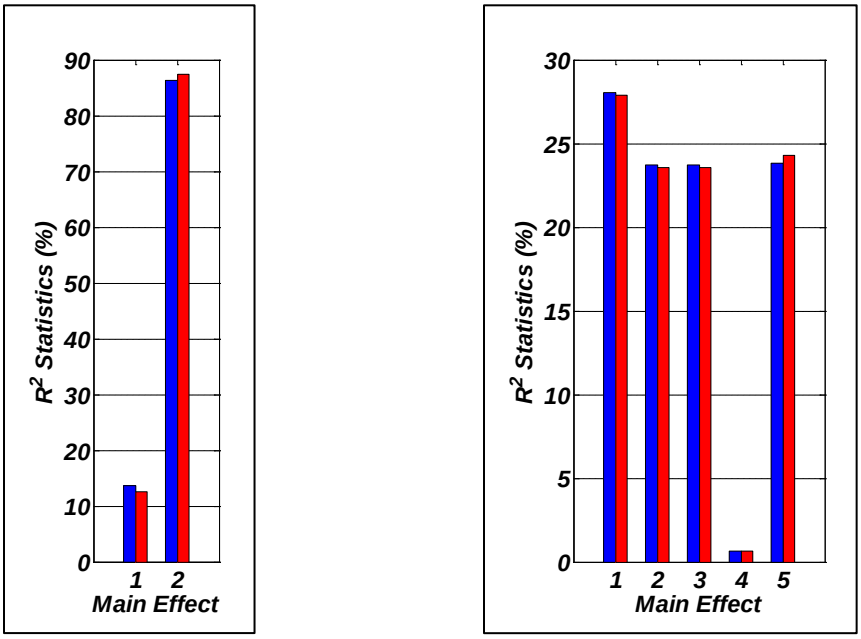

Figure 19: Results of main effects analysis from varying BISON gap heat transfer (left) and fuel relocation (right) parameters

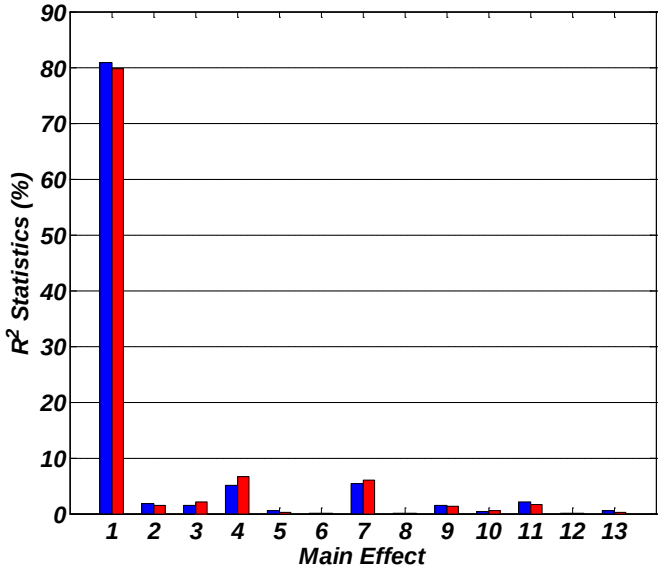

Figure 20: Results of main effects analysis from varying BISON thermal conductivity parameters

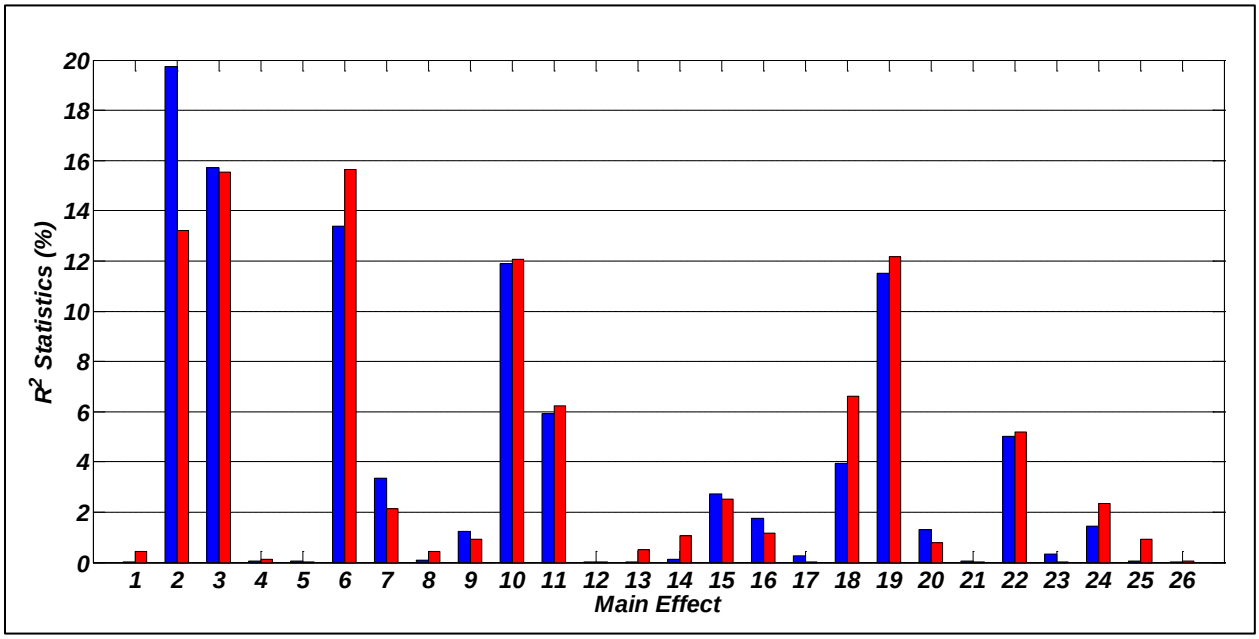

Figure 21: Results of main effects analysis from varying BISON fission gas release parameters

Going beyond the main effects analyses presented above, a more thorough analysis is also conducted, leading to the final list of parameters presented in Table 24. First, ANOVA models are constructed that include both main effects *and* linear interactions for each set of results, organized by physics model (*e.g.* fission gas release). Next, a stepwise procedure is employed to

reduce the order of the fitted model using the Akaike Information Criterion, in order to avoid overfitting. This final model is then examined and parameters are selected that contribute substantially to explaining the output variability, either as main effects or as linear interactions (or both); note that this process is performed for both features of interest. For the last step, while it is true that statistical significance was used as a guide, but it is not necessarily true that all statistically significant parameters were chosen. In one case for example, a variable (CONTACT_COEFF) was selected because it had a larger effect size than the other variable in the model, but it was *not* statistically significant in the main effects model.

Table 24: Parameters varied for the sensitivity analysis conducted on the BISON fuel performance code

Parameter Number	**Model Name**	**Parameter Name**
1	Fuel Relocation	FUEL_RELOC_1
2		FUEL_RELOC_2
3		FUEL_RELOC_3
4		FUEL_RELOC_5
5	Gap Heat Transfer	CONTACT_COEFF
6	Fission Gas Release	GR_GRAIN_RAD
7		GR_RESOL_RATE
8		GR_RESOL_DEPTH
9		GR_BUBBLE_RAD
10		GR_BUBBLE_SHAPE_FACT
11		GR_SURF_TENSION
12		GR_FRAC_COVERAGE
13		GR_FRAC_YIELD
14		GR_CALIB_FACTOR
15		DC_FRAG_INFLUENCE
16		DC_GAS_ATOM_DIFF_COEFF_1
17		DC_GAS_ATOM_DIFF_COEFF_4
18		DC_GAS_ATOM_DIFF_COEFF_5
19		DC_INTRA_BUBBLE_RAD_3
20		DC_INTRA_CAPTURE_RATE
21		DC_INTRA_RESOL_RATE
22	Thermal Conductivity	FINK_EQN19_1
23		FINK_EQN19_4
24		LUCUTA_EQN7a
25		LUCUTA_EQN11b

6 Conclusion

This report represents a collection of three methodologies aimed at assessing the predictive capability of the empirical thermal conductivity model adopted by the nuclear fuel performance code, FRAPCON-3.4. The first of these methodologies adopted an optimization-based approach, by way of a genetic algorithm, to infer the optimal model parameters for predicting thermal conductivity data associated with the fresh and irradiated fuel samples, separately. While much insight was gained as to the behavior of the models with respect to the available data, the primary conclusion was that the thermal conductivities associated with the fresh fuel samples could *not* be accurately predicted when employing the data / model from the irradiated fuel samples.

This result was confirmed and expounded upon by the second methodology that adopted a Bayesian approach to infer posterior probabilities of the parameters by way of Markov Chain Monte Carlo (MCMC) analyses. The unique facet of this approach was that it considered the *simultaneous* calibration of the two models to all of the available data, which served to confirm the hypothesis that independent calibration of the models / data should be done with caution, especially when considering the model / data associated with the irradiated fuel samples. The issues associated with this model (*i.e.* Equation (8)) lead the authors to question whether or not the model is of the correct mathematical form. As noted in Section 1.1, many authors have proposed variants of Equation (8), all of which have fit the available data to one degree or another. Therefore, future efforts will focus on addressing this issue, possibly by proposing a model that departs from Equation (8), so as to better predict the overall behavior exhibited by the available data.

The third and final methodology adopted *Info-Gap Decision Theory* (IGDT) to explore a relatively new concept for quantifying uncertainty of empirically-derived models: *info-gap robustness*. Info-gap robustness, in essence, quantifies the sensitivities of a model to parametric uncertainty, without relying on approximations of global or local derivatives (or adjoints). Furthermore, this uncertainty quantification is performed within the context of a performance metric and yields an intuitive mechanism (*i.e.* the robustness curve) by which analysts may both understand and convey the effects of parametric uncertainties in their model. Generally speaking, the conclusions drawn from this effort were consistent with those of the other two methodologies. However, one of the distinguishing characteristics of the analyses was the unique way in which the results were framed.

The final section of this report offered a preliminary assessment of Idaho National Laboratory's nuclear fuel performance code, BISON. A large number of code execution failures produced by varying the parameters associated with the six models selected for this study yielded somewhat inconclusive results. Future BISON-focused studies will attempt to address the issues that likely impacted the progress of this preliminary assessment, keeping in mind that further development of the code may be the simplest means by which to generate the desired results.

Acknowledgements

This work was sponsored by the U.S. Department of Energy, Nuclear Energy Division, Advanced Modeling and Simulation Office (NE-71), Nuclear Energy Advanced Modeling and Simulation (NEAMS) Program, Verification, Validation and Uncertainty Quantification (VU) program element. The authors are grateful to Dr. Keith Bradley, NEAMS national Technical Director, Mr. James Peltz, NEAMS Program Manager, Dr. Robert Versluis, NEAMS Program Manager, Mr. Alex Larzelere, Director of the Advanced Modeling and Simulation Office, and Dr. James Stewart, NEAMS VU Technical Lead, for their support. Los Alamos National Laboratory is operated by the Los Alamos National Security, LLC for the National Nuclear Security Administration of the U.S. Department of Energy under contract DE-AC52-06NA25396.

References

[1] Ronchi C, Sheindlin M, Staicu D, Kinoshita M. Effect of burn-up on the thermal conductivity of uranium dioxide up to 100.000 MWd/t. Journal of Nuclear Materials. 2004; 327: p. 58-76.

[2] Fink JK. Thermophysical properties of uranium dioxide. Journal of Nuclear Materials. 2000; 279: p. 1-18.

[3] Lucuta PG, Matzke H, Hastings IJ. A pragmatic approach to modelling thermal conductivity of irradiated UO2 fuel: review and recommendations. Journal of Nuclear Materials. 1996; 232: p. 166-180.

[4] Ohira , Itagaki. Thermal conductivity measurements of high burnup UO2 pellet and a benchmark calculation of fuel center temperature. In Proceedings of the ANS International Topical Meeting on LWR Fuel Performance; 1997; Portland. p. 541-9.

[5] Williamson RL, Hales JD, Novascone SR, Tonks MR, Gaston DR, Permann CJ, et al. Multidimensional multiphysics simulation of nuclear fuel behavior. Journal of Nuclear Materials. 2012 April; 423(1-3): p. 149-63.

[6] Gaston D, Newman C, Hansen G, Lebrun-Grandie D. MOOSE: A parallel computational framework for coupled systems of nonlinear equations. Nuclear Engineering and Design. 2009 October; 239(10): p. 1768-78.

[7] Hemez FM, Atamturktur HS, Unal C. Defining predictive maturity for validated numerical simulations. Technical Report LA-UR-08-06741. Los Alamos National Laboratory; 2008.

[8] Stull CJ, Hemez FM, Williams BJ, Unal C, Rogers ML. An improved description of predictive maturity for verification and validation activities. Technical Report LA-UR-11-05659. Los Alamos: Los Alamos National Laboratory; 2011.

[9] Oberkampf WL, Pilch M, Trucano TG. Predictive capability maturity model for computational modeling and simulation. Technical Report SAND2007-5948. Albuquerque: Sandia National Laboratories; 2007.

[10] Mitchell M. An Introduction to Genetic Algorithms Cambridge: The MIT Press; 1998.

[11] The MathWorks, Inc. MATLAB R2012a Product Help. Natick; 2012.

[12] Graves TL. Automatic step size selection in random walk Metropolis algorithms. 2011. arXiv:1103.5986v1 [stat.CO].

[13] Gilks WR, Richardson S, Spiegelhalter DJ. Markov Chain Monte Carlo in Practice Boca Raton: Chapman & Hall; 1996.

[14] Ben-Haim Y. Info-Gap Decision Theory: Decisions Under Severe Uncertainty. 2nd ed. Oxford: Academic Press; 2006.

[15] Stull CJ, Hemez FM. On the use of info-gap decision theory to select from among models of varying complexity. Technical Report LA-UR-12-00379. Los Alamos: Los Alamos National Laboratory; 2012.

[16] Ben-Haim Y. Info-Gap Decision Theory: Decisions Under Severe Uncertainty. [Online].; 2012 [cited 2012 September 12. Available from: http://info-gap.com/.

[17] Geelhood KJ, Luscher WG, Beyer CE. FRAPCON-3.4: A computer code for the calculation of steady-state thermal-mechanical behavior of oxide fuel rods for high burnup. Technical Report NUREG/CR-7022. Washington, DC: U.S. Nuclear Regulatory Commission; 2011.

[18] Lanning DD, Beyer CE, Berna GA. FRAPCON-3: Integral Assessment. Technical Report NUREG/CR-6534. Washington, DC: U.S. Nuclear Regulatory Commission; 1997.

[19] Christensen JA, et al.. Uranium Dioxide thermal conductivity. Transactions of the American Nuclear Society. 1964; 7: p. 391-2.

[20] Godfrey TG, et al.. Thermal conductivity of Uranium Dioxide and Armco Iron by an improved radiant heat flow technique. Technical Report ORNL-3556. Oak Ridge: Oak Ridge National Laboratory; 1964.

[21] Bates JL. High temperature thermal conductivity of “round robin” Uranium Dioxide. Technical Report BNWL-1431. Richland: Battelle Northwest Laboratory; 1970.

[22] Gibby RL. The effect of Plutonium content on the thermal conductivity of (U,Pu)O2 solid solutions. Journal of Nuclear Materials. 1971; 38: p. 163-77.

[23] Weilbacher JC. Diffusivite thermique de l’Oxyde d’Uranium et de l’Oxyde de Thorium a haute temperature. High Temperatures--High Pressure. 1972; 4: p. 431-8.

[24] Hobson IC, Taylor R, Ainscough JB. Effect of porosity and stoichiometry on the thermal

conductivity of Uranium Oxide. Journal of Physics Section D: Applied Physics. 1974; 7: p. 1003-15.

[25] Ronchi C, Sheindlin M, Musella M, Hyland GJ. Thermal conductivity of uranium dioxide up to 2900 K from simultaneous measurement of the heat capacity and thermal diffusivity. Journal of Applied Physics. 1999 January 15; 85(2): p. 776-89.

[26] Goldsmith LA, Douglas JAM. Measurements of the thermal conductivity of Uranium Dioxide at 670-1270K. Journal of Nuclear Materials. 1973; 47: p. 31-42.

[27] Beyer CE, Lanning DD. Review of thermal conductivity data and models. In Proceedings of the Seminar on Thermal Performance of High Burn-up LWR Fuel; 1998; Cadarache: Organisation for Economic Co-operation and Development (OECD) Nuclear Energy Agency (NEA). p. 57-70.

[28] Amaya M, Hirai M, Sakurai H, Ito K, Sasaki M, Nomata T, et al. Thermal conductivities of irradiated UO2 and (U,Gd)O2 pellets. Journal of Nuclear Materials. 2002; 2002: p. 57-64.

Appendix A – Experimental Data from Fresh Fuel Samples

In the following tables, the captions refer to "% TD;" this is percent of theoretical density.

Table A-25: Conductivity data from Christensen et al. [19], % TD = 94.0%

Temperature, K	**K_{exp}, W/m-K**
1312.00	2.87
1389.00	2.87
1432.00	2.70
1496.00	2.72
1552.00	2.71
1587.00	2.56
1612.00	2.57
1656.00	2.80
1747.00	2.48
1838.00	2.59

Table A-26: Conductivity data from Godfrey et al. [20], % TD = 93.4%

Temperature, K	**K_{exp}, W/m-K**		**Temperature, K**	**K_{exp}, W/m-K**
574.00	5.40		570.00	5.14
673.00	4.75		572.00	5.11
767.00	4.32		673.00	4.59
877.00	3.90		673.00	4.56
976.00	3.56		774.00	4.08
1074.00	3.27		774.00	4.10
675.00	4.61		875.00	3.71
870.00	3.79		875.00	3.73
869.00	3.83		973.00	3.42
971.00	3.49		973.00	3.42
1072.00	3.18		1071.00	3.17
1165.00	2.99		1071.00	3.16
1173.00	2.98		1173.00	2.95
1279.00	2.77		1271.00	2.75
1282.00	2.76		1323.00	2.68
572.00	5.19		576.00	5.23
870.00	3.74		576.00	5.23
870.00	3.69		671.00	4.69
872.00	3.68		671.00	4.69
1171.00	2.89		671.00	4.71
1175.00	2.87		874.00	3.82

Table A-27: Conductivity data from Bates [21], % TD = 98.4%

Temperature K	**K_{exp} W/m-K**		**Temperature K**	**K_{exp} W/m-K**
539.00	6.50		2102.00	2.25
539.00	6.57		2174.00	2.26
756.00	4.82		2187.00	2.25
761.00	5.02		2373.00	2.49
895.00	4.11		2373.00	2.64
891.00	4.35		2280.00	2.29
994.00	3.83		2285.00	2.42
995.00	3.91		1599.00	2.37
1180.00	3.28		1601.00	2.49
1185.00	3.13		1609.00	2.32
1325.00	2.85		1360.00	2.83
1325.00	2.89		1453.00	2.42
1489.00	2.51		1562.00	2.48
1491.00	2.55		1649.00	2.37
1666.00	2.40		1750.00	2.39
1655.00	2.37		1907.00	2.13
1778.00	2.24		2005.00	2.10
1780.00	2.13		2007.00	2.31
1863.00	2.19		2109.00	2.19
1866.00	2.19		2104.00	2.27
1977.00	2.10		2195.00	2.35
1972.00	2.24		2295.00	2.47
2093.00	2.32		2384.00	2.42

Table A-28: Conductivity data from Bates [21], % TD = 98.4%

Temperature K	**K_{exp} W/m-K**		**Temperature K**	**K_{exp} W/m-K**
571.00	5.72		1270.00	2.80
577.00	6.03		1269.00	2.87
577.00	6.16		1270.00	2.81
661.00	5.33		1361.00	2.55
682.00	5.41		1361.00	2.63
786.00	4.48		1361.00	2.59
784.00	4.45		1361.00	2.63
785.00	4.54		1471.00	2.54
866.00	4.15		1472.00	2.67
867.00	4.15		1469.00	2.26
961.00	3.73		1569.00	2.40
961.00	3.63		1571.00	2.41
961.00	3.96		1569.00	2.46
1069.00	3.35		1683.00	2.33
1071.00	3.31		1683.00	2.37
1069.00	3.51		1758.00	2.30
1171.00	3.04		1756.00	2.19
1174.00	3.07		1760.00	2.28
1173.00	3.24			

Table A-29: Conductivity data from Bates [21], % TD = 98.4%

Temperature K	**Kexp W/m-K**		**Temperature K**	**Kexp W/m-K**
673.00	5.53		678.00	5.33
1283.00	2.75		776.00	4.88
673.00	5.42		775.00	4.96
1100.00	3.60		891.00	4.17
1089.00	3.40		895.00	4.30
1090.00	3.54		968.00	3.88
1099.00	3.41		973.00	3.96
813.00	4.86		1087.00	3.45
797.00	4.80		1081.00	3.48
507.00	6.46		1172.00	3.28
583.00	6.40		1173.00	3.16
676.00	5.42		1292.00	2.85
679.00	5.51		1291.00	2.81
763.00	5.01		1377.00	2.65
764.00	5.13		1380.00	2.63
873.00	4.50		1473.00	2.54
876.00	4.29		1477.00	2.59
979.00	3.95		1578.00	2.30
981.00	3.96		1584.00	2.45
1065.00	3.74		1673.00	2.23
1072.00	3.69		1679.00	2.20
1188.00	3.17		1769.00	2.09
1187.00	3.36		1792.00	2.24
1277.00	3.09		1786.00	2.19
1285.00	3.19		1595.00	2.06
1284.00	3.28		1596.00	2.41
1071.00	3.70		1400.00	2.61
880.00	4.57		1399.00	2.56
879.00	4.52		1166.00	3.29
879.00	4.52		1079.00	3.44
678.00	5.34		1085.00	3.50
573.00	6.18		847.00	4.43
583.00	5.89		847.00	4.45
680.00	5.36		577.00	5.98
681.00	5.24		553.00	6.22

Table A-30: Conductivity data from Gibby [22], % TD = 95.8%

Temperature K	**K_{exp} W/m-K**		**Temperature K**	**K_{exp} W/m-K**
575.00	6.24		1031.00	3.94
578.00	6.36		1031.00	3.84
586.00	6.28		1071.00	3.66
587.00	5.87		1080.00	3.47
588.00	5.63		1080.00	3.55
665.00	5.12		1204.00	3.24
675.00	5.20		1204.00	3.34
679.00	5.31		1280.00	3.13
690.00	5.12		1288.00	2.99
846.00	4.30		1288.00	2.92
846.00	4.40		1289.00	2.99
852.00	4.53		1323.00	3.01
853.00	4.65		1335.00	2.90
865.00	4.30		1384.00	2.92
865.00	4.40		1390.00	2.80
893.00	4.29		1395.00	2.70
908.00	4.29		1399.00	2.80
907.00	4.20		1412.00	2.95
964.00	3.84		1491.00	2.78
964.00	3.92		1502.00	2.44
969.00	4.02		1508.00	2.62
969.00	4.12		1510.00	2.66
1000.00	3.70			

Table A-31: Conductivity data from Weilbacher [23], % TD = 98.0%

Temperature K	**K_{exp} W/m-K**		**Temperature K**	**K_{exp} W/m-K**
974.00	3.58		2284.00	2.45
974.00	3.81		2379.00	2.45
1171.00	3.09		2379.00	2.54
1171.00	3.25		2484.00	2.61
1377.00	2.62		2483.00	2.73
1376.00	2.85		2577.00	2.74
1575.00	2.31		2577.00	2.86
1575.00	2.51		2674.00	2.91
1778.00	2.18		2674.00	3.02
1776.00	2.39		2773.00	3.10
1979.00	2.19		2773.00	3.21
1980.00	2.33		2875.00	3.32
2180.00	2.26		2875.00	3.44
2182.00	2.39		3025.00	3.66
2281.00	2.31		3027.00	3.83

Table A-32: Conductivity data from Hobson et al. [24], % TD = 94.9%

Temperature K	**K_{exp} W/m-K**		**Temperature K**	**K_{exp} W/m-K**
547.00	5.76		1500.00	2.81
607.00	5.41		1532.00	2.84
642.00	5.33		1621.00	2.63
732.00	4.96		1638.00	2.69
788.00	4.63		1749.00	2.52
834.00	4.45		1760.00	2.58
885.00	4.26		1807.00	2.46
944.00	4.13		1871.00	2.60
995.00	4.01		1913.00	2.48
1046.00	3.86		1993.00	2.45
1083.00	3.75		2016.00	2.52
1133.00	3.62		2059.00	2.47
1150.00	3.51		2154.00	2.43
1175.00	3.53		2154.00	2.49
1279.00	3.23		2243.00	2.47
1330.00	3.15		2336.00	2.51
1392.00	3.04		2412.00	2.63
1449.00	2.97		2503.00	2.66

Table A-33: Conductivity data from Ronchi et al. [25], % TD = 95.0%

Temperature K	**K_{exp} W/m-K**		**Temperature K**	**K_{exp} W/m-K**
568.00	5.23		761.00	4.15
569.00	5.02		771.00	4.03
572.00	4.99		772.00	4.06
572.00	4.93		772.00	4.00
575.00	4.88		773.00	4.00
577.00	4.97		776.00	4.00
578.00	4.94		791.00	3.92
586.00	5.06		807.00	3.98
611.00	4.72		823.00	3.90
611.00	4.78		826.00	3.87
612.00	4.72		845.00	3.78
612.00	4.72		845.00	3.72
613.00	4.78		846.00	3.69
613.00	4.72		861.00	3.78
614.00	4.69		880.00	3.67
614.00	4.69		893.00	3.64
614.00	4.72		902.00	3.61
614.00	4.75		903.00	3.58
614.00	4.72		911.00	3.62
614.00	4.75		925.00	3.53
614.00	4.78		938.00	3.50
615.00	4.75		953.00	3.44
615.00	4.69		978.00	3.33
615.00	4.72		981.00	3.33
615.00	4.69		989.00	3.33
615.00	4.69		1010.00	3.28
615.00	4.72		1032.00	3.25
615.00	4.75		1051.00	3.20
621.00	4.76		1081.00	3.15
668.00	4.60		1889.00	1.92
674.00	4.51		1997.00	2.21
687.00	4.37		1998.00	2.07
689.00	4.37		2020.00	2.03
690.00	4.58		2059.00	2.02
691.00	4.34		2060.00	1.87
712.00	4.44		2094.00	1.93
728.00	4.23		2095.00	1.79
732.00	4.23		2122.00	2.13
737.00	4.21		2123.00	2.12
738.00	4.24		2147.00	2.21
750.00	4.15		2178.00	2.46

Table A-34: Conductivity data from Ronchi et al. [25] (continued), % TD = 95.0%

Temperature K	**K_{exp} W/m-K**
2180.00	2.40
2197.00	2.19
2197.00	2.16
2238.00	2.18
2268.00	2.11
2268.00	2.14
2272.00	1.82
2299.00	2.24
2299.00	2.29
2355.00	1.96
2394.00	2.02
2394.00	2.18
2396.00	2.44
2425.00	2.00
2429.00	2.01
2438.00	1.98
2438.00	2.37
2456.00	2.28
2457.00	2.22
2500.00	2.35
2500.00	2.23
2500.00	2.26
2501.00	1.98
2504.00	2.11
2545.00	2.59
2561.00	1.99
2623.00	2.21
2628.00	2.26
2632.00	2.53
2634.00	2.08
2638.00	2.21
2640.00	2.13
2669.00	2.38
2672.00	2.43
2677.00	2.48
2682.00	2.59
2768.00	2.68
2782.00	2.48
2786.00	2.87
2802.00	2.77
2873.00	2.79

Table A-35: Conductivity data from Goldsmith and Douglas [26], % TD = 90.5%

Temperature K	**K_{exp} W/m-K**
670.00	4.20
870.00	3.49
1070.00	2.91
1270.00	2.46
670.00	4.40
870.00	3.69
1070.00	3.10
1270.00	2.59

Table A-36: Conductivity data from Goldsmith and Douglas [26], % TD = 93.1%

Temperature K	**K_{exp} W/m-K**
670.00	4.61
870.00	3.88
1070.00	3.30
1270.00	2.75
670.00	4.55
870.00	3.80
1070.00	3.24
1270.00	2.66

Table A-37: Conductivity data from Goldsmith and Douglas [26], % TD = 94.7%

Temperature K	**K_{exp} W/m-K**
670.00	5.08
870.00	4.26
1070.00	3.61
1270.00	3.01

Table A-38: Conductivity data from Goldsmith and Douglas [26], % TD = 95.2%

Temperature K	**K_{exp} W/m-K**
670.00	4.85
870.00	4.16
1070.00	3.46
1270.00	2.95

Table A-39: Conductivity data from Goldsmith and Douglas [26], % TD = 95.8%

Temperature K	**K_{exp} W/m-K**
670.00	4.98
870.00	4.10
1070.00	3.56
1270.00	3.01

Table A-40: Conductivity data from Goldsmith and Douglas [26], % TD = 96.0%

Temperature K	**K_{exp} W/m-K**
670.00	5.57
670.00	5.19
870.00	4.38
1070.00	3.70
1270.00	3.12

Table A-41: Conductivity data from Goldsmith and Douglas [26], % TD = 97.7%

Temperature K	**K_{exp} W/m-K**
670.00	5.43
870.00	4.60
1070.00	3.87
1270.00	3.23

Table A-42: Conductivity data from Goldsmith and Douglas [26], % TD = 98.2%

Temperature K	**K_{exp} W/m-K**
670.00	5.31
870.00	4.44
1070.00	3.75
1270.00	3.16

Table A-43: Conductivity data from Goldsmith and Douglas [26], % TD = 98.6%

Temperature K	**K_{exp} W/m-K**
670.00	5.53
670.00	5.59
870.00	4.68
870.00	4.67
870.00	4.70
1070.00	3.96
1070.00	3.94
1070.00	3.94
1270.00	3.27
1270.00	3.26
1270.00	3.32

Appendix B – Experimental Data from Irradiated Fuel Samples

In the following tables, the captions refer to "% TD" and "% BU;" these are percent of theoretical density and percent burn-up, respectively.

Table B-44: Conductivity data from Lucuta et al. [3], % TD = 94.0%, % BU = 65.366%

Temperature K	**K_{exp} W/m-K**
631.21	2.96
676.40	2.85
720.27	2.79
773.71	2.69
827.20	2.63
883.45	2.59
937.00	2.59
983.65	2.56
1041.28	2.53
1087.93	2.50
1142.82	2.46
1188.08	2.42
1236.07	2.36
1281.36	2.34
1330.73	2.28
1478.93	2.21

Table B-45: Conductivity data from Lucuta et al. [3], % TD = 94.0%, % BU = 65.366%

Temperature K	**K_{exp} W/m-K**
631.44	3.19
719.06	2.95
775.21	2.81
828.66	2.72
882.09	2.60
939.75	2.60
980.94	2.60
1039.92	2.54
1092.05	2.50
1141.44	2.46
1236.10	2.39
1286.87	2.36
1332.16	2.34
1385.67	2.31
1477.63	2.27

Table B-46: Conductivity data from Lucuta et al. [3], % TD = 86.0%, % BU = 65.366%

Temperature K	**K_{exp} W/m-K**
606.48	2.18
675.38	2.13
730.51	2.08
792.52	2.05
842.11	2.05
894.48	2.02
937.19	2.02
989.55	1.99
1037.77	1.99
1091.50	2.00
1143.83	2.07
1187.90	2.13
1243.01	2.13
1299.50	2.12
1350.48	2.11
1398.70	2.10
1451.07	2.05
1499.30	2.04
1554.41	2.02
1606.78	1.97

Table B-47: Conductivity data from Lucuta et al. [3], % TD = 86.0%, % BU = 65.366%

Temperature K	**K_{exp} W/m-K**
605.06	2.30
675.35	2.22
729.10	2.16
793.87	2.12
842.12	2.05
895.86	2.01
941.32	2.02
989.55	1.99
1043.28	2.00
1095.63	2.00
1146.59	2.07
1193.41	2.13
1241.62	2.15
1298.12	2.12
1353.22	2.13
1400.08	2.10
1452.44	2.07
1500.67	2.06
1555.79	2.02
1608.15	1.98

Table B-48: Conductivity data from Beyer and Lanning [27], % TD = 96.0%, % BU = 63.000%

Temperature K	**K_{exp} W/m-K**
294.29	3.46
374.29	3.64
474.29	3.52
574.29	3.24
671.43	2.99
774.29	2.84
871.43	2.71

Table B-49: Conductivity data from Beyer and Lanning [27], % TD = 86.0%, % BU = 63.000%

Temperature K	**K_{exp} W/m-K**
286.04	2.11
351.77	2.17
423.20	2.18
548.88	2.07
660.28	1.97
771.68	1.86
874.54	1.88

Table B-50: Conductivity data from Lucuta et al. [3], % TD = 95.3%, % BU = 40.000%

Temperature K	**K_{exp} W/m-K**
676.26	2.77
835.85	2.60
1073.23	2.42
1273.11	2.25
1471.63	2.13
1674.29	1.96

Table B-51: Conductivity data from Lucuta et al. [3], % TD = 95.3%, % BU = 40.000%

Temperature K	**K_{exp} W/m-K**
676.31	2.53
876.00	2.35
1072.97	2.21
1272.79	2.11
1472.61	2.01
1675.03	1.80

Table B-52: Conductivity data from Ronchi et al. [1], % TD = 95.0%, % BU = 34.000%

Temperature K	**K_{exp} W/m-K**
500.00	2.93
550.00	2.85
600.00	2.77
650.00	2.69
700.00	2.62
750.00	2.55
800.00	2.47
850.00	2.40
900.00	2.34
950.00	2.29
1000.00	2.24
1050.00	2.20
1100.00	2.15
1150.00	2.10
1200.00	2.05
1250.00	1.97
1300.00	1.92
1350.00	1.90
1400.00	1.90
1450.00	1.90

Table B-53: Conductivity data from Ronchi et al. [1], % TD = 95.0%, % BU = 34.000%

Temperature K	**K_{exp} W/m-K**
500.00	3.13
550.00	3.00
600.00	2.88
650.00	2.78
700.00	2.68
750.00	2.58
800.00	2.50
850.00	2.41
900.00	2.34
950.00	2.27
1000.00	2.25
1050.00	2.16
1100.00	2.04
1150.00	1.98
1200.00	1.91
1250.00	1.90
1300.00	1.87
1350.00	1.85
1400.00	1.80
1450.00	1.80

Table B-54: Conductivity data from Ronchi et al. [1], % TD = 95.0%, % BU = 33.000%

Temperature K	**K_{exp} W/m-K**
500.00	3.09
550.00	2.97
600.00	2.85
650.00	2.75
700.00	2.65
750.00	2.56
800.00	2.47
850.00	2.39
900.00	2.32
950.00	2.24
1000.00	2.18
1050.00	2.12
1100.00	2.06
1150.00	2.00
1200.00	1.95
1250.00	1.88
1300.00	1.85
1350.00	1.82
1400.00	1.78
1450.00	1.74

Table B-55: Conductivity data from Ronchi et al. [1], % TD = 95.0%, % BU = 34.000%

Temperature K	**K_{exp} W/m-K**
500.00	3.12
550.00	2.97
600.00	2.84
650.00	2.73
700.00	2.62
750.00	2.51
800.00	2.42
850.00	2.33
900.00	2.25
950.00	2.18
1000.00	2.11
1050.00	2.04
1100.00	1.98
1150.00	1.92
1200.00	1.86
1250.00	1.81
1300.00	1.76
1350.00	1.72
1400.00	1.67
1450.00	1.63

Table B-56: Conductivity data from Ronchi et al. [1], % TD = 95.0%, % BU = 55.000%

Temperature K	**K_{exp} W/m-K**
500.00	2.41
550.00	2.36
600.00	2.32
650.00	2.27
700.00	2.23
750.00	2.19
800.00	2.15

Table B-57: Conductivity data from Ronchi et al. [1], % TD = 95.0%, % BU = 51.000%

Temperature K	**K_{exp} W/m-K**
500.00	2.68
550.00	2.60
600.00	2.52
650.00	2.45
700.00	2.38
750.00	2.31
800.00	2.25
850.00	2.19
900.00	2.13
950.00	2.08
1000.00	2.02
1050.00	1.96
1100.00	1.91
1150.00	1.87
1200.00	1.82
1250.00	1.78
1300.00	1.75
1350.00	1.72
1400.00	1.69
1450.00	1.68

Table B-58: Conductivity data from Ronchi et al. [1], % TD = 95.0%, % BU = 51.000%

Temperature K	**K_{exp} W/m-K**
500.00	2.44
550.00	2.37
600.00	2.32
650.00	2.26
700.00	2.21
750.00	2.16
800.00	2.11
850.00	2.06
900.00	2.02
950.00	1.98
1000.00	1.94
1050.00	1.90
1100.00	1.86
1150.00	1.83
1200.00	1.80
1250.00	1.79
1300.00	1.79
1350.00	1.78
1400.00	1.77
1450.00	1.77

Table B-59: Conductivity data from Ronchi et al. [1], % TD = 95.0%, % BU = 51.000%

Temperature K	**K_{exp} W/m-K**
500.00	3.46
550.00	3.30
600.00	3.15
650.00	3.01
700.00	2.88
750.00	2.77
800.00	2.66
850.00	2.56
900.00	2.47
950.00	2.38
1000.00	2.30
1050.00	2.23
1100.00	2.16
1150.00	2.09
1200.00	2.03
1250.00	1.97
1300.00	1.92
1350.00	1.87
1400.00	1.82
1450.00	1.77

Table B-60: Conductivity data from Ronchi et al. [1], % TD = 95.0%, % BU = 82.000%

Temperature K	**K_{exp} W/m-K**
500.00	2.18
550.00	2.16
600.00	2.14
650.00	2.12
700.00	2.10
750.00	2.08
800.00	2.07

Table B-61: Conductivity data from Ronchi et al. [1], % TD = 95.0%, % BU = 96.000%

Temperature K	**K_{exp} W/m-K**
500.00	2.06
550.00	2.04
600.00	2.03
650.00	2.01
700.00	1.99
750.00	1.97
800.00	1.95

Table B-62: Conductivity data from Ronchi et al. [1], % TD = 95.0%, % BU = 92.000%

Temperature K	**K_{exp} W/m-K**
500.00	2.50
550.00	2.42
600.00	2.34
650.00	2.27
700.00	2.20
750.00	2.14
800.00	2.08
850.00	2.02
900.00	1.97
950.00	1.92
1000.00	1.87
1050.00	1.82
1100.00	1.78
1150.00	1.74
1200.00	1.70
1250.00	1.66
1300.00	1.62
1350.00	1.59
1400.00	1.56
1450.00	1.52

Table B-63: Conductivity data from Ohira and Itagaki [4], % TD = 95.0%, % BU = 60.976%

Temperature K	**K_{exp} W/m-K**
675.00	2.25
873.00	2.25
873.00	2.16
874.00	2.09
1075.00	2.14
1075.00	2.12
1271.00	2.12
1270.00	2.08
1272.00	2.01
1475.00	2.01
1473.00	1.96
1474.00	1.88
1669.00	1.95
1673.00	1.83
1672.00	1.77

Table B-64: Conductivity data from Amaya et al. [28], % TD = 96.5%

Temperature K	**K_{exp} W/m-K**	**% BU**
1273	2.72	8.294
1273	2.64	8.294
1273	2.54	16.674
1273	2.40	38.963
1273	2.59	42.333
1273	2.37	44.406
1273	2.43	48.553
1273	2.23	49.849
1273	2.27	52.959
1273	2.04	55.724
1273	2.31	59.698
1273	2.99	0.000

Appendix C – Supplemental Data from GA Optimization Analyses

Below are presented the experimental data / model prediction comparison plots and parameter tables for the GA optimization analyses, allowing ten percent deviation from the nominal parameter values, associated with Sections 2.2.1 and 2.2.2.

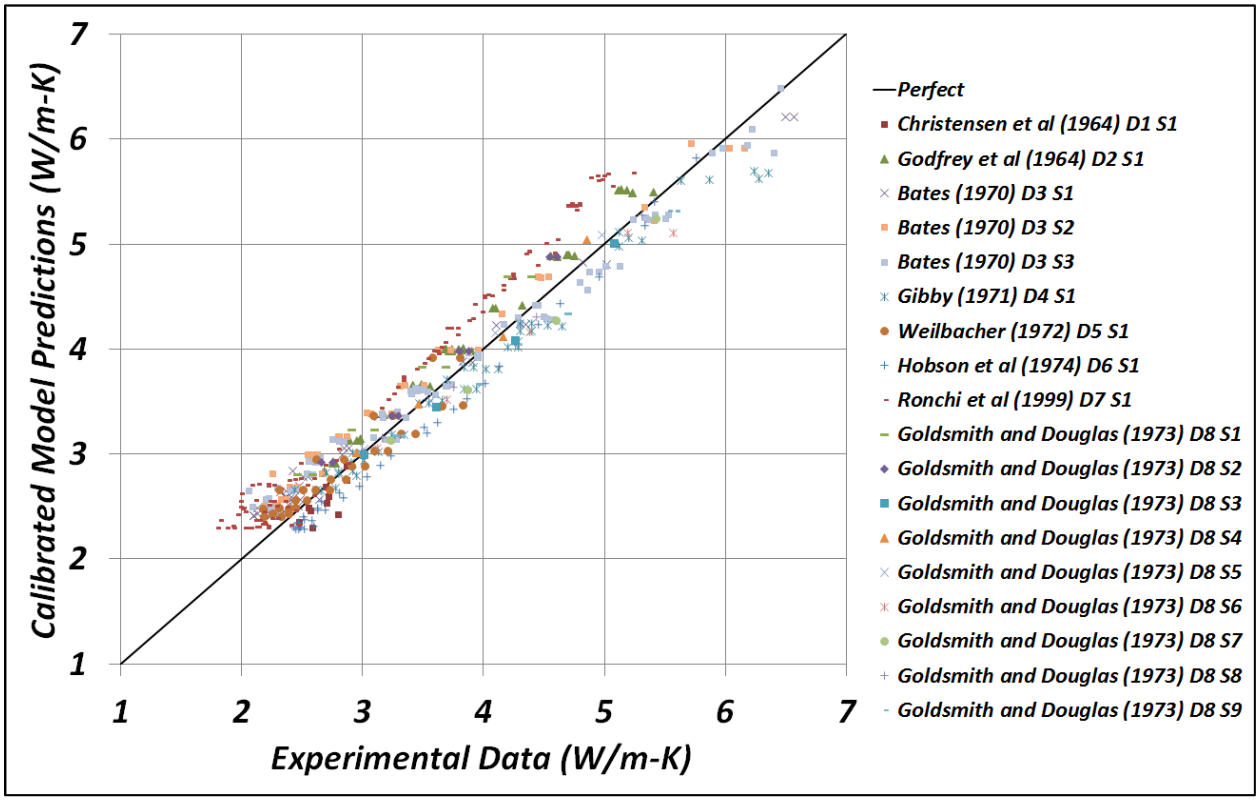

Figure C-22: Comparison between experimental data and **GA-optimized** model predictions for thermal conductivity, allowing **10%** deviation from the nominal parameter values

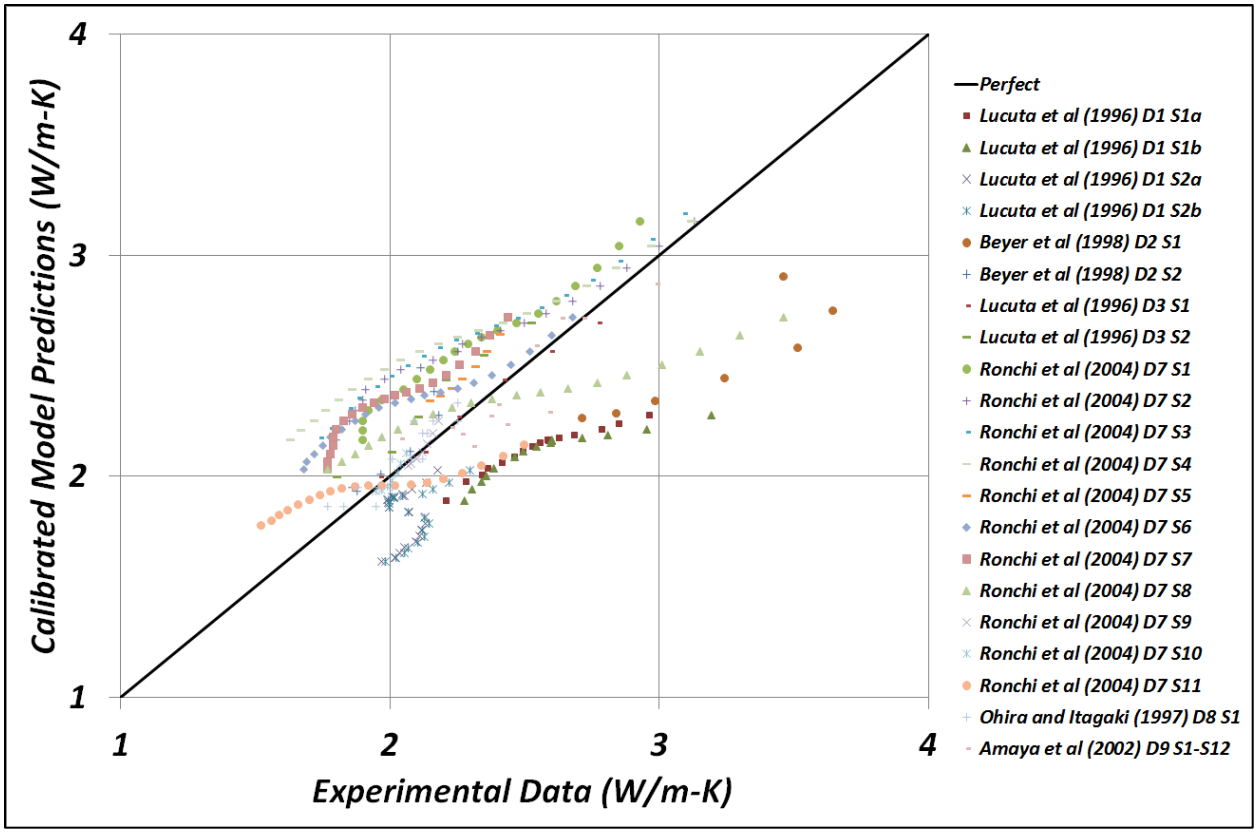

Figure C-23: Comparison between experimental data and **GA-optimized** model predictions for thermal conductivity, allowing **10%** deviation from the nominal parameter values

Table C-65: GA-optimized parameter values, allowing **10%** deviation from the nominal parameter values

Parameter Name	**Nominal Value**	**GA-Optimized Value**	**Relative Difference (%)**
A (m-K/W)	0.0452	0.04972	10.0%
B (m-K/W/K)	0.000246	0.0002420	1.6%
E (W-K/m)	3.50E+09	3.156E+09	9.8%
F (K)	16361	15649.3	4.4%
f(Bu)	0.00187	0.001683	10.0%
0.9 Factor	0.9	0.810	10.0%
0.04 Factor	0.04	0.0440	10.0%
g(Bu) A	0.038	0.0418	10.0%
g(Bu) B	0.28	0.273	2.6%
h(T)	396	435.6	10.0%
Q	6380	5916.4	7.3%

Table C-66: GA-optimized parameter values, allowing **50%** deviation from the nominal parameter values (bold entries denote parameters that are held fixed at the values given in Table 4)

Parameter Name	**Nominal Value**	**GA-Optimized Value**	**Relative Difference (%)**
***A* (m-K/W)**	**0.0452**	**0.04889**	**8.2%**
***B* (m-K/W/K)**	**0.000246**	**0.0002400**	**8.9%**
***E* (W-K/m)**	**3.50E+09**	**3.850E+09**	**10.0%**
***F* (K)**	**16361**	**16296.4**	**0.4%**
f(Bu)	0.00187	0.000991	47.0%
0.9 Factor	0.9	0.450	50.0%
0.04 Factor	0.04	0.060	50.0%
$g(Bu)_A$	0.038	0.0570	50.0%
$g(Bu)_B$	0.28	0.2749	1.8%
h(T)	396	198.4	49.9%
Q	6380	6584.3	3.2%

Table C-67: GA-optimized parameter values, allowing **10%** deviation from the nominal parameter values (bold entries denote parameters that are held fixed at the values given in Table 4)

Parameter Name	Nominal Value	GA-Optimized Value	Relative Difference (%)
***A* (m-K/W)**	**0.0452**	**0.04889**	**8.2%**
***B* (m-K/W/K)**	**0.000246**	**0.0002400**	**8.9%**
***E* (W-K/m)**	**3.50E+09**	**3.850E+09**	**10.0%**
***F* (K)**	**16361**	**16296.4**	**0.4%**
f(Bu)	0.00187	0.001683	10.0%
0.9 Factor	0.9	0.810	10.0%
0.04 Factor	0.04	0.044	10.0%
$g(Bu)_A$	0.038	0.0418	10.0%
$g(Bu)_B$	0.28	0.2828	1.0%
h(T)	396	356.4	10.0%
Q	6380	6792.8	6.5%

Appendix D – Supplemental Data from MCMC Analyses

This section presents the results of ten MCMC analyses in which some data sets were held out from the analysis (as opposed to the analyses presented in Section 3, in which all data sets were included). A total of ten, randomly selected data sets were held out from each of the ten analyses: five data sets associated with the fresh fuel samples and five data sets associated with the irradiated fuel samples. The data sets held out from each analysis are given in Table D-68.

Table D-68: Data sets held out from each of the ten "Holdout Cases"

	HC-1	**HC-2**	**HC-3**	**HC-4**	**HC-5**	**HC-6**	**HC-7**	**HC-8**	**HC-9**	**HC-10**
Fresh Fuel Samples	1	2	1	7	2	2	2	4	1	6
	7	4	3	8	4	4	13	7	5	7
	10	6	9	9	5	7	14	8	6	9
	16	7	10	12	11	10	15	13	13	12
	18	15	13	16	14	16	16	18	18	13
Irradiated Fuel Samples	3	11	3	3	5	1	3	4	2	2
	5	15	4	14	8	5	5	6	5	11
	6	17	5	15	9	6	11	8	15	12
	14	19	12	17	13	14	12	10	18	16
	16	20	20	21	18	21	21	11	20	19

Table D-69 presents, for each of the ten "Holdout Cases," the average RMS errors associated with each data set, after the calibration has been conducted using the remaining twenty-nine data sets (*i.e.* those *not* listed in Table D-68). Generally speaking, the average RMS errors presented in Table D-69 demonstrate that holding out data from the calibration does not dramatically degrade the quality of the calibrated models. Figure D-24 through Figure D-33 present the posteriors (univariate and bivariate) for each of the ten "Holdout Cases." Comparing these results to the right panel of Figure 10, further confirms that the authors' assertion that the calibrated models do not deviate dramatically from that generated by employing all thirty-nine data sets.

Table D-69: Average RMS error for each data set, for each the ten "Holdout Cases"

	HC-1	**HC-2**	**HC-3**	**HC-4**	**HC-5**	**HC-6**	**HC-7**	**HC-8**	**HC-9**	**HC-10**
Fresh Fuel Samples	0.30	0.09	0.25	0.21	0.10	0.11	0.09	0.18	0.29	0.27
	0.33	0.22	0.15	0.35	0.24	0.21	0.12	0.35	0.35	0.12
	0.17	0.40	0.45	0.37	0.31	0.34	0.12	0.39	0.45	0.42
	0.39	0.34	0.28	0.21	0.09	0.20	0.39	0.13	0.19	0.21
	0.42	0.43	0.13	0.32	0.12	0.35	0.38	0.43	0.50	0.13
Irradiated Fuel Samples	0.34	0.22	0.38	0.34	0.60	0.52	0.33	0.34	0.56	0.55
	0.64	0.30	0.39	0.18	0.09	0.63	0.63	0.30	0.61	0.22
	0.25	0.23	0.64	0.27	0.13	0.25	0.18	0.09	0.24	0.28
	0.15	0.14	0.20	0.22	0.26	0.15	0.24	0.16	0.19	0.35
	0.33	0.09	0.14	0.28	0.20	0.28	0.26	0.18	0.11	0.17
Avg (HC)	0.33	0.25	0.30	0.27	0.21	0.30	0.27	0.26	0.35	0.27
Avg (No HC)	0.22	0.27	0.22	0.24	0.27	0.23	0.24	0.26	0.24	0.23

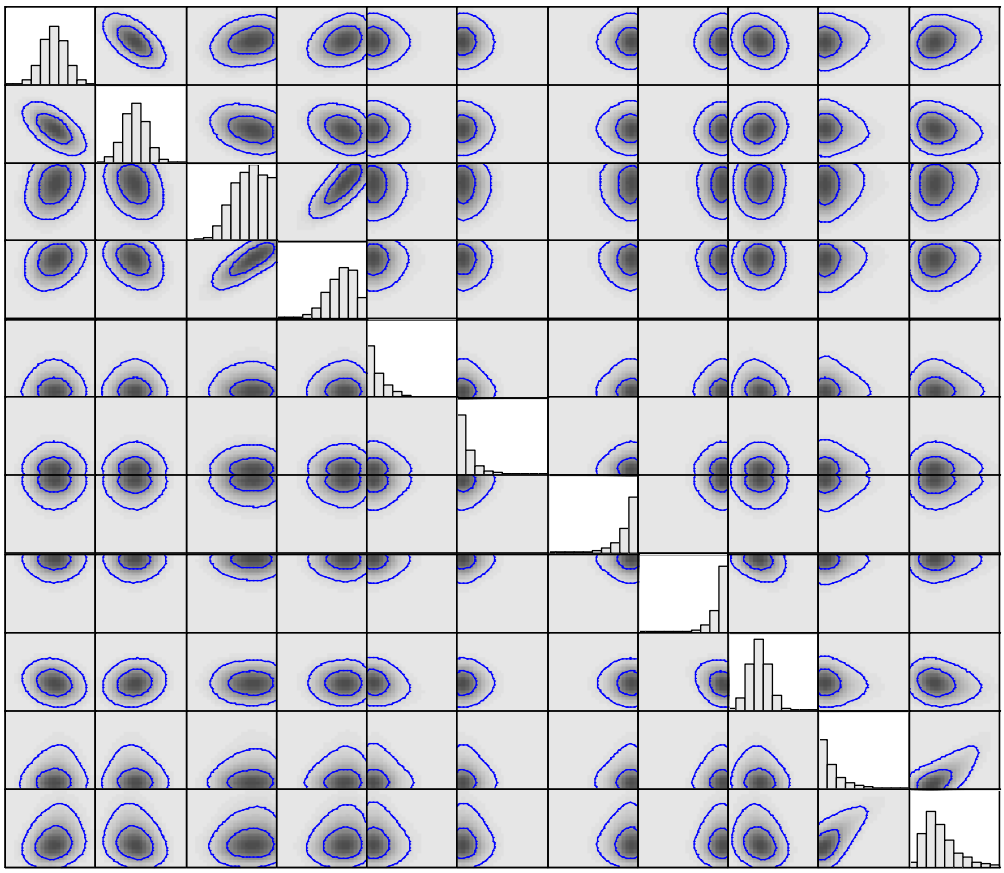

Figure D-24: Estimates of univariate (diagonal) and bivariate (off-diagonal) marginal posterior distributions for Holdout Case 1

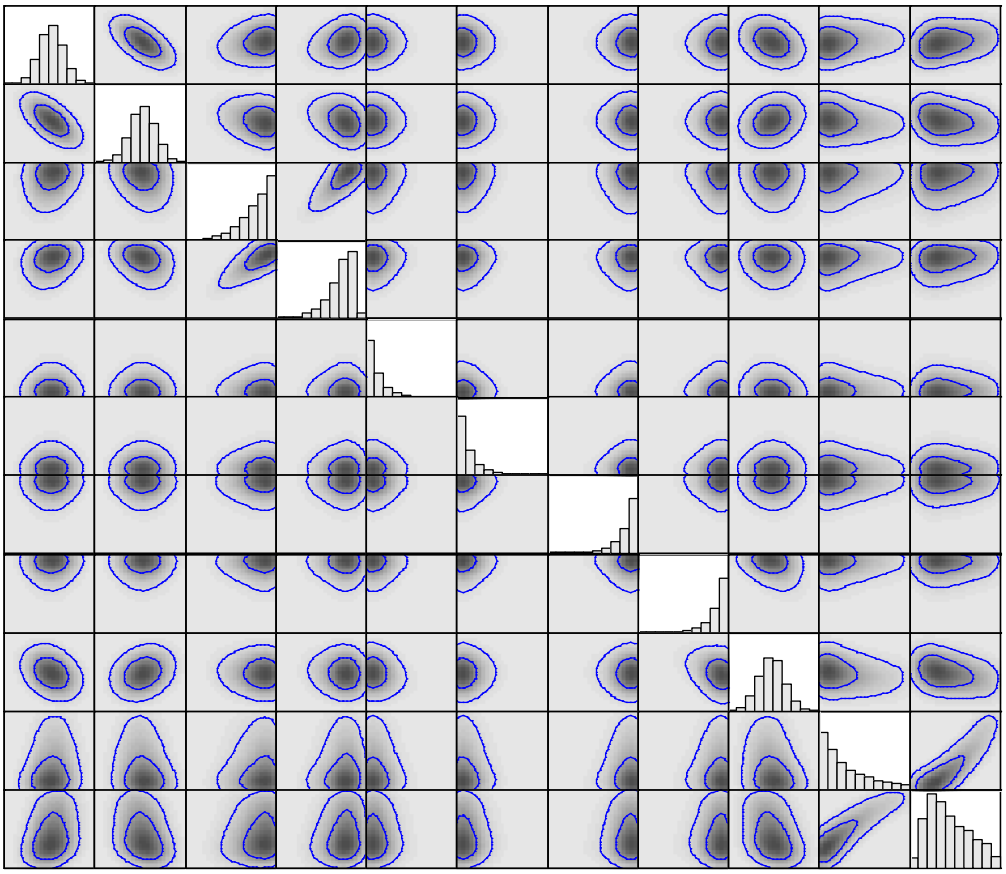

Figure D-25: Estimates of univariate (diagonal) and bivariate (off-diagonal) marginal posterior distributions for Holdout Case 2

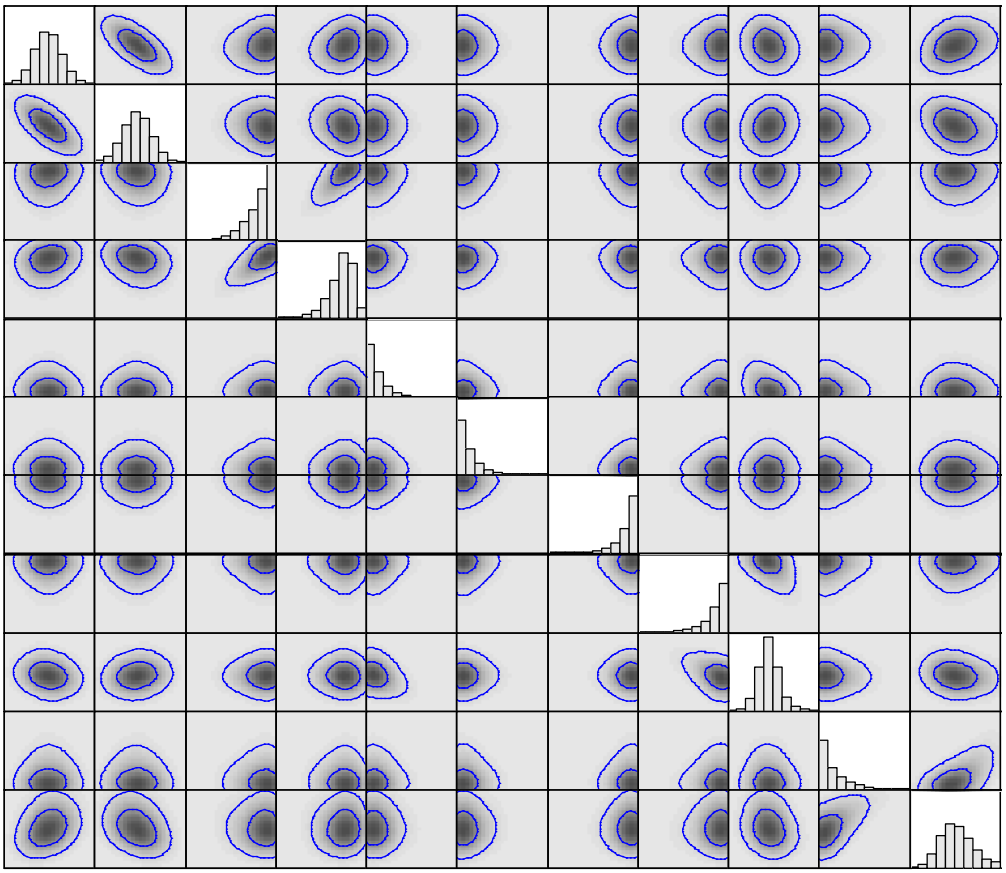

Figure D-26: Estimates of univariate (diagonal) and bivariate (off-diagonal) marginal posterior distributions for Holdout Case 3

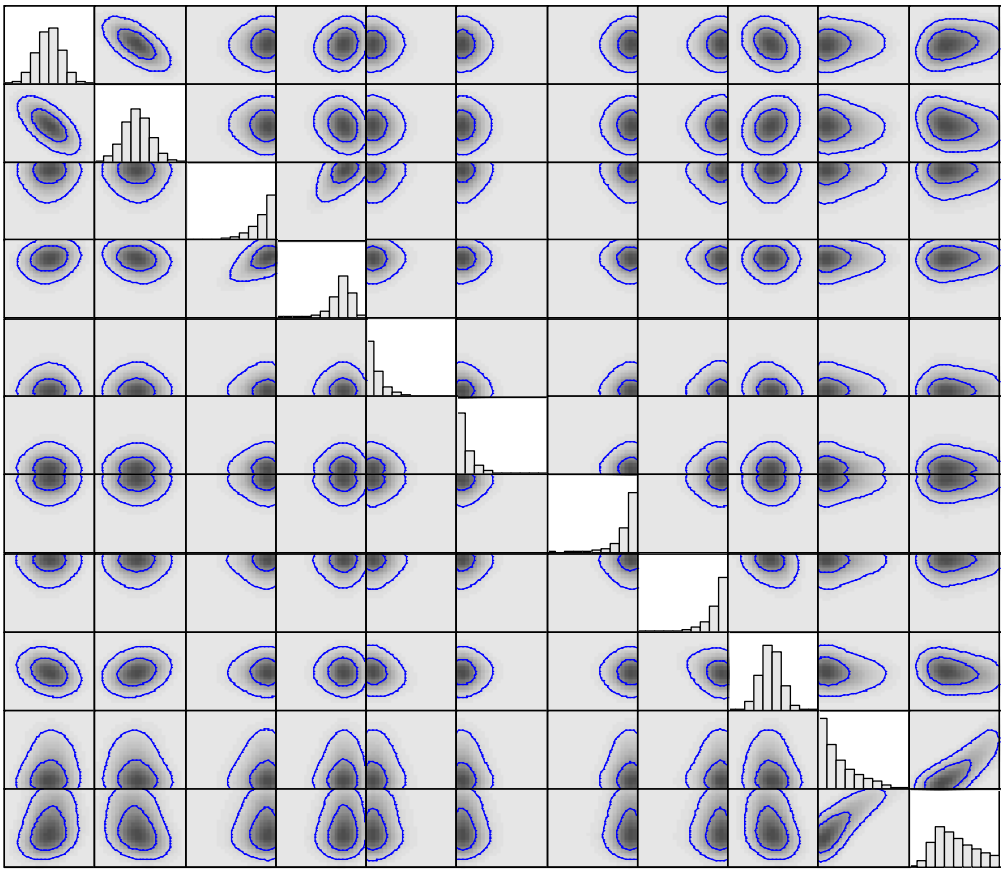

Figure D-27: Estimates of univariate (diagonal) and bivariate (off-diagonal) marginal posterior distributions for Holdout Case 4

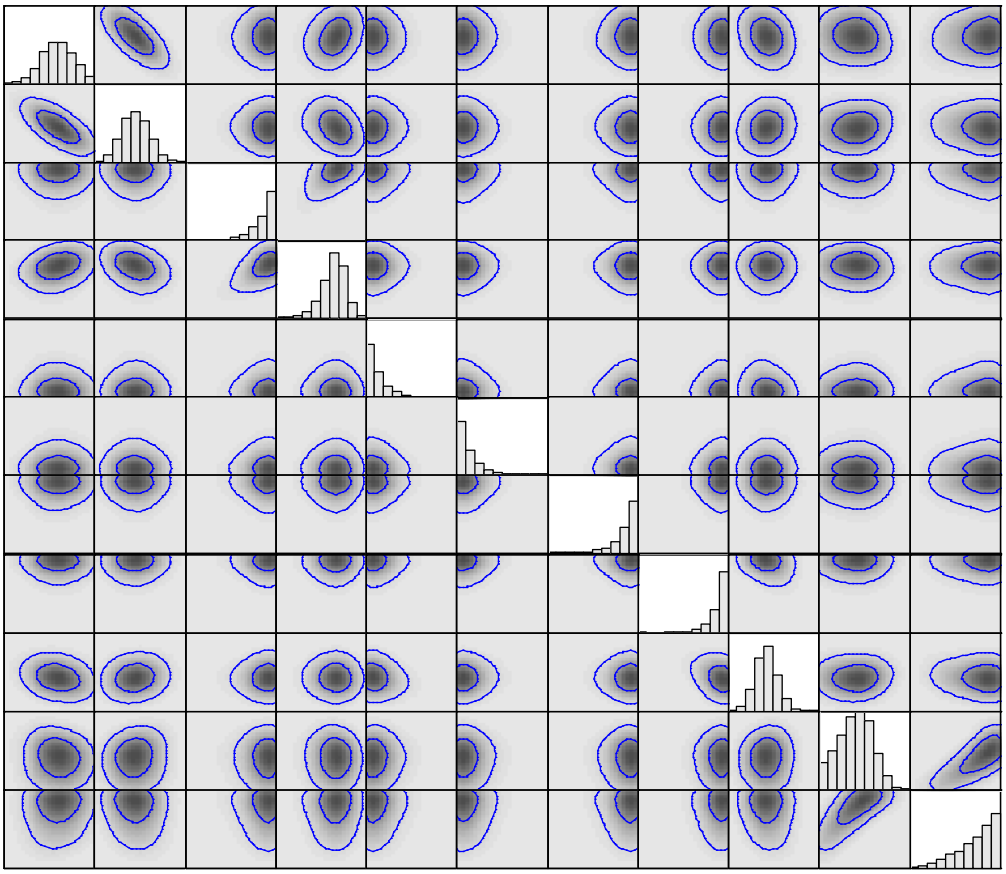

Figure D-28: Estimates of univariate (diagonal) and bivariate (off-diagonal) marginal posterior distributions for Holdout Case 5

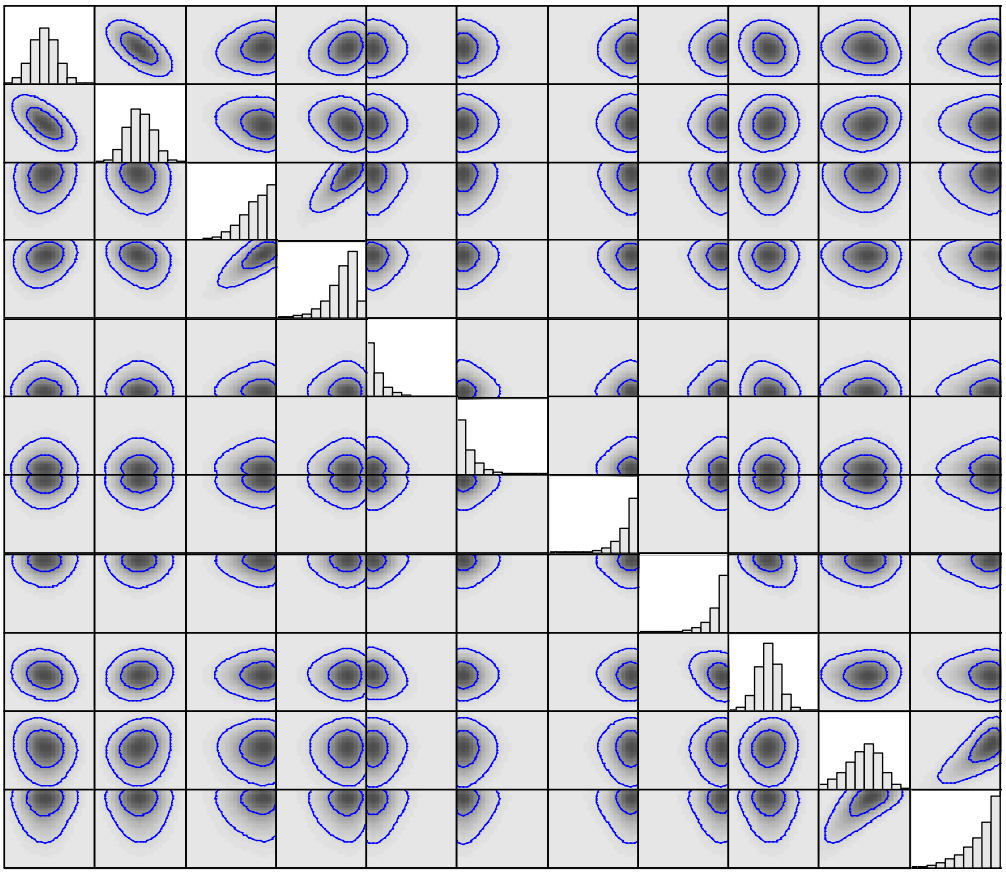

Figure D-29: Estimates of univariate (diagonal) and bivariate (off-diagonal) marginal posterior distributions for Holdout Case 6

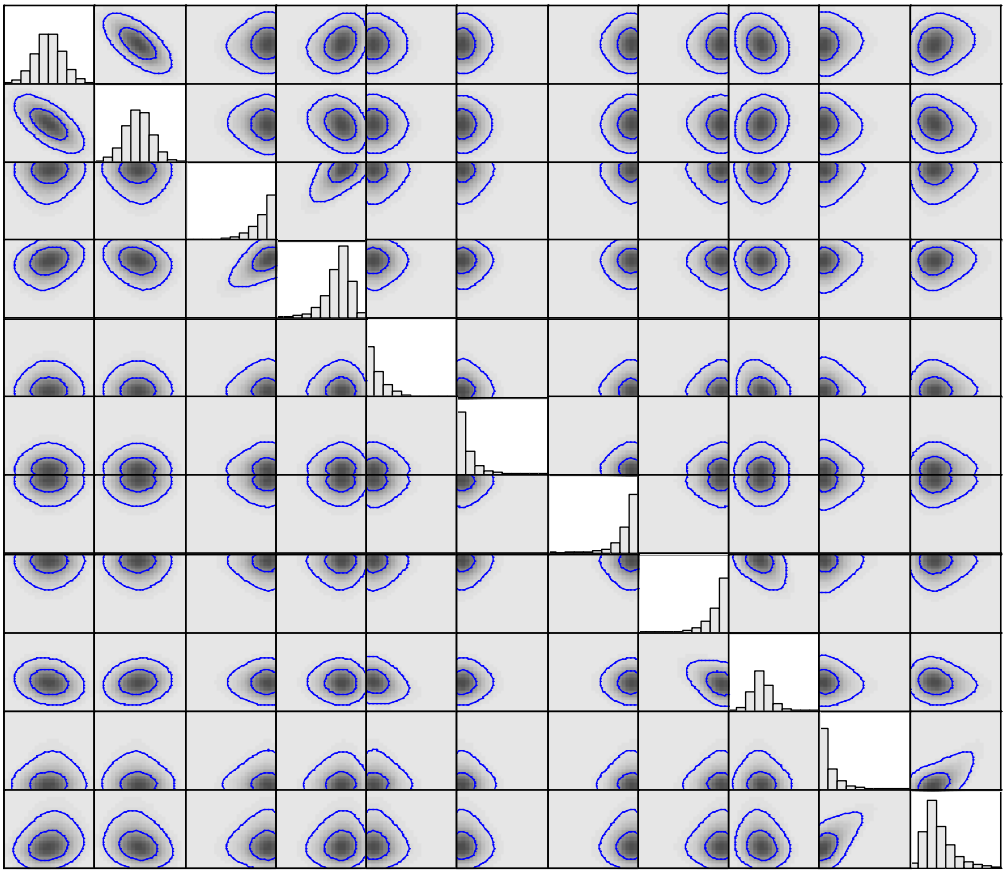

Figure D-30: Estimates of univariate (diagonal) and bivariate (off-diagonal) marginal posterior distributions for Holdout Case 7

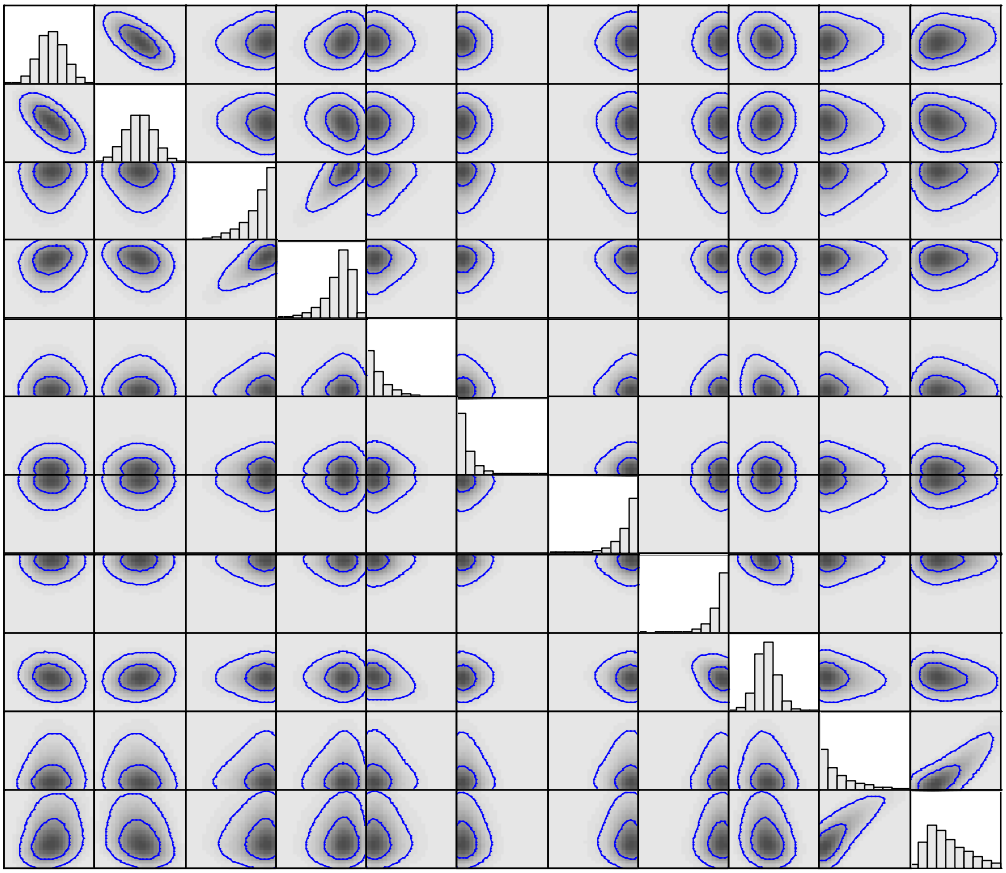

Figure D-31: Estimates of univariate (diagonal) and bivariate (off-diagonal) marginal posterior distributions for Holdout Case 8

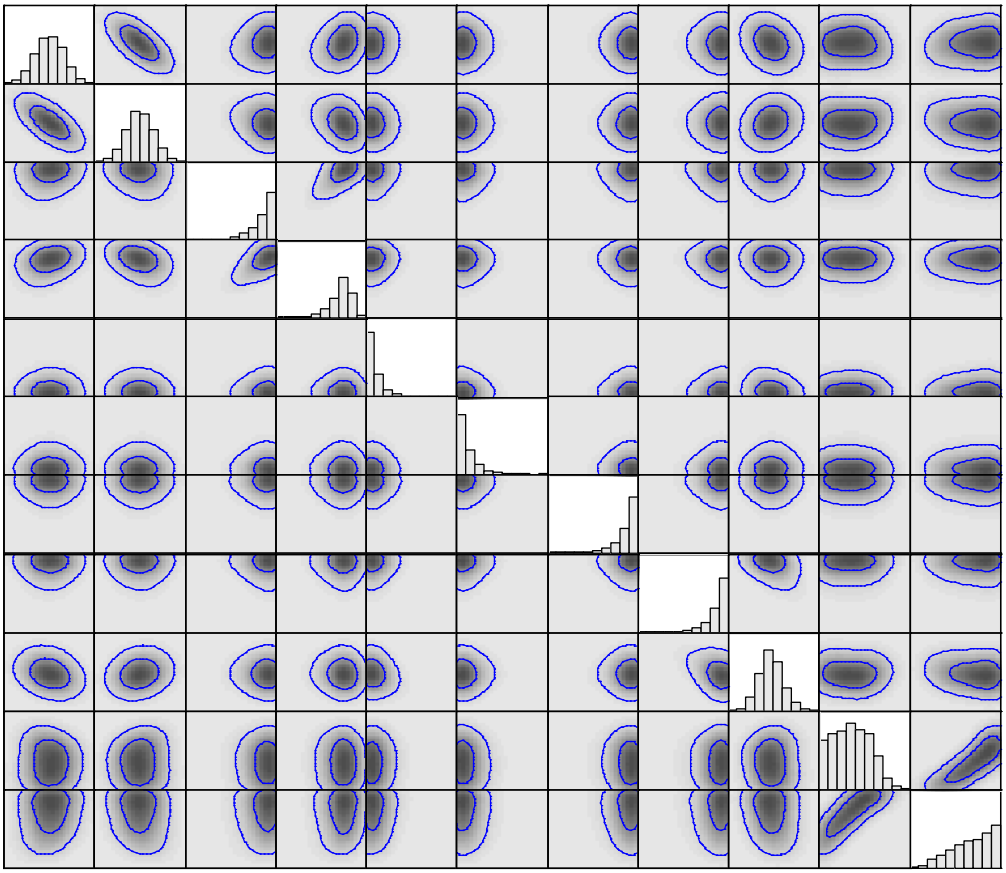

Figure D-32: Estimates of univariate (diagonal) and bivariate (off-diagonal) marginal posterior distributions for Holdout Case 9

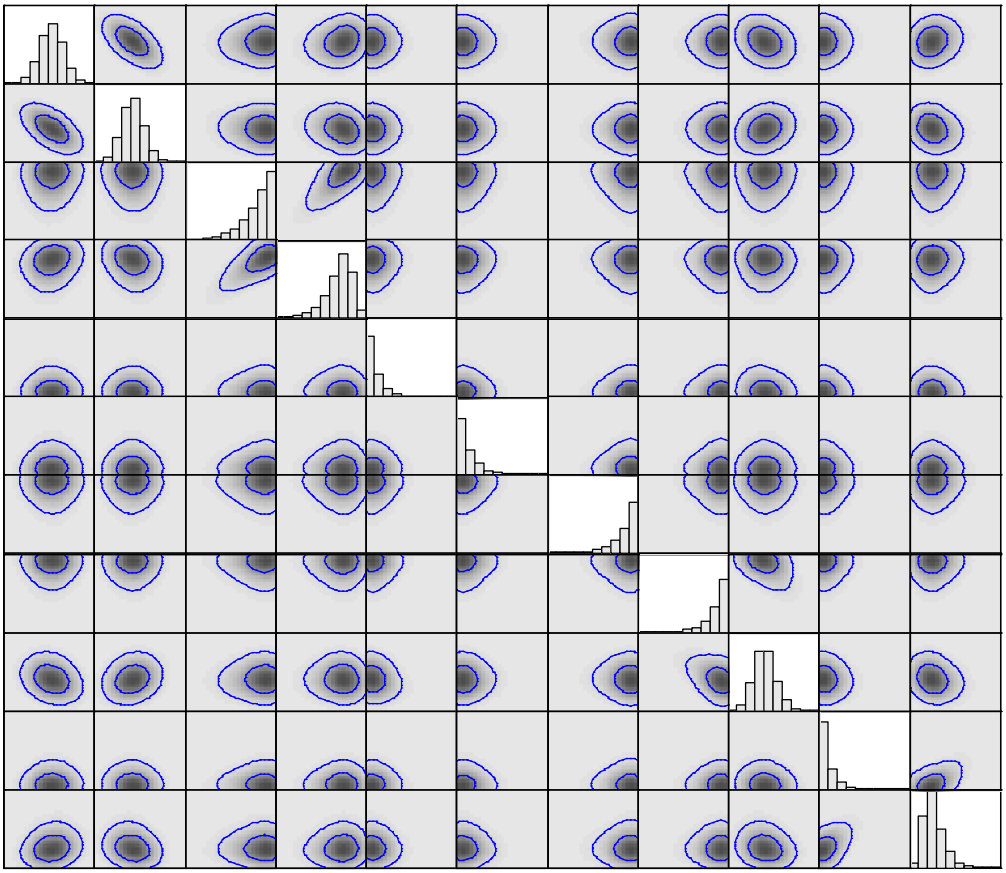

Figure D-33: Estimates of univariate (diagonal) and bivariate (off-diagonal) marginal posterior distributions for Holdout Case 10

Appendix E – Supplemental Data from IGDT Analyses

Below are presented the influence curves from the follow-on IGDT analyses associated with Sections 4.2.1 and 4.2.2.

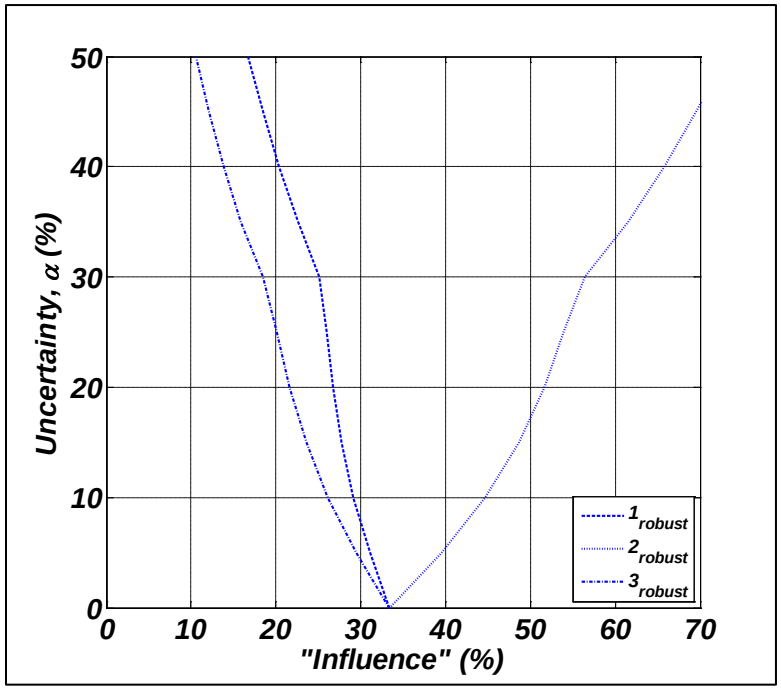

Figure E-34: Influence curves from the **three**-parameter case

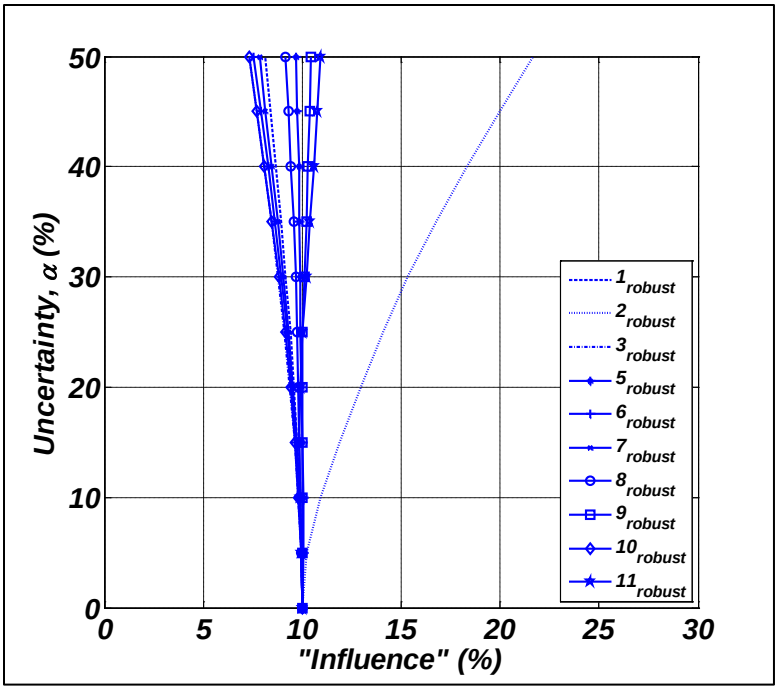

Figure E-35: Influence curves from the **ten**-parameter case